Spring 1-1-2017

Design and Qualication of an Upstream Gust Generator in a Low-Speed Wind Tunnel

Daniel Gretz Bateman
University of Colorado at Boulder, dangbateman@yahoo.com

Design and Qualification of an Upstream Gust Generator in a Low-Speed Wind Tunnel

by

Daniel Bateman

B.S., Lehigh University, 2015

A thesis submitted to the

Faculty of the Graduate School of the

University of Colorado in partial fulfillment

of the requirements for the degree of

Master of Science

Ann and H.J. Smead Department of Aerospace Engineering Sciences

2017

This thesis entitled:
Design and Qualification of an Upstream Gust Generator in a Low-Speed Wind Tunnel
written by Daniel Bateman
has been approved for the Ann and H.J. Smead Department of Aerospace Engineering Sciences

Prof. John Farnsworth

Prof. John Evans

Prof. Kenneth Jansen

Date

The final copy of this thesis has been examined by the signatories, and we find that both the content and the form meet acceptable presentation standards of scholarly work in the above mentioned discipline.

Bateman, Daniel (M.S., Aerospace Engineering)

Design and Qualification of an Upstream Gust Generator in a Low-Speed Wind Tunnel

Thesis directed by Prof. John Farnsworth

A longitudinal gust generator was designed, constructed, installed and tested in the low-speed research wind tunnel within the Experimental Aerodynamics Laboratory at University of Colorado Boulder. The system consists of a dynamic shutter (louver) system composed ten airfoil vanes geared together in five counter-rotation pairs which was installed at the wind tunnel inlet. By dynamically adjusting the angle of the airfoil vanes, the inlet area was rapidly varied from 0 to 85% blocked area. After installation, a quasi-static evaluation of the system was performed to determine the relationship between inlet area blocked by the airfoil vanes and reduction of test section velocity. It was found that the test section speed could be reduced to around 50% of the fully open test section speed. Once the static qualification was completed, the vanes were dynamically opened and closed to create time-varying gusts in the test section (longitudinal) velocity. The velocity response of the tunnel was quantified using a combination of three hotwire anemometers distributed throughout the test section. Several types of gust profiles were created including: (1) continuous sinusoidal oscillations of the free stream velocity magnitude, (2) discrete impulses, and (3) linear ramps. Using hotwires at different points in the test section, the speed at which disturbances traveled through the tunnel was measured. The wind tunnel was found to have two distinct time responses, a faster time response for decelerating the flow, and a slower time response for accelerating the flow. The speeds at which the disturbances propagated through the test section was at least an order of magnitude higher than the freestream velocity for all speeds and types of pulses tested. This suggests that the disturbances behave globally with a closed test section.

Acknowledgements

I would first and foremost like to thank Prof. John Farnsworth for his guidance and leadership. Without his dedication to this project, this would not have been possible.

I would also like to acknowledge everyone involved in the extensive amount of construction in this project. Thank you to Adrian Stang and Matt Rhode, of the Aerospace Machine shop, for not only helping me from brainstorming through manufacturing, but also for teaching me the many of the skills I learned along the way. I would also like to thank Severyn Polakiewicz for his assistance in designing this system.

I would like to acknowledge the other members of the Experimental Aerodynamics Lab, Ethan, Joseph, and Lucas. Thank you for your insight, guidance, and sense of humor. Finally, I would like to thank my family for their love and support throughout this entire process.

Contents

Chapter

Tables

Table

Figures

Figure

Chapter 1

Introduction

For the last 75 years, unsteady wind tunnel facilities have played a crucial role in understanding the many aspects of unsteady aerodynamics. Recently, several facilities have been built due to the desire to research environments for micro aerial vehicles (MAVs) and unmanned aerial vehicles (UAVs). The work carried out by these facilities goes well beyond just UAVs and MAVs and includes research in aeroelasticity and aircraft gust response.

Most of this research has been motivated, directly or indirectly, by atmospheric gusts. The atmosphere presents a naturally unsteady environment for flying vehicles. Realizing the importance of gusts in the development of aircraft, the National Advisory Council on Aeronautics (NACA) issued the first gust loading requirements for aircraft in 1934[14]. This inspired the creation of the first unsteady wind tunnel facility shortly thereafter. Since then, multiple facilities have been developed which are capable of producing various types of gusts or unsteadiness. This abundance of experimentation has created a solid foundation of knowledge surrounding the field of unsteady aerodynamics, but with new technologies emerging, there is still a need to continue research in this area.

1.1 Established work and Facilities

This section will attempt to provide a brief overview of some of the many unsteady flow facilities, as well as describing motivation for their construction. There are three intuitive ways of imposing unsteadiness on a model: (1) a change in motion of the working fluid, (2) a change in

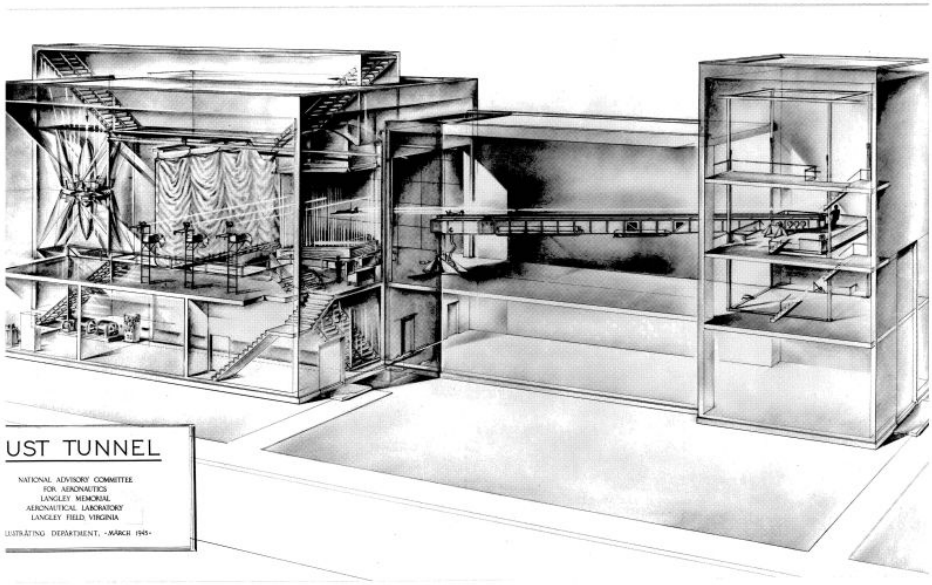

Figure 1.1: The gust generator facility at Langley, 1945 [4]

motion of the model being tested, and (3) a combination of fluid and model motion. Facilities have been constructed in each of these three categories, each with their own advantages and limitations.

1.1.1 Model and Fluid Motion

Despite the relative complexity of this type of system, the first unsteady wind tunnel test facility used this concept. After NACA issued the first set of gust loading requirements for aircraft design, a pilot test facility was proposed at the Langley Research Facility. Following the success of the pilot tunnel, a larger structure was built for this purpose as pictured in Figure 1.1. Both the pilot facility and the larger facility followed the same concept. Using a catapult, a model plane was accelerated into steady flight in calm air before passing into a transverse gust region. The gust region was created by a blower, and could be varied in size, shape and strength. The model was then arrested by a set of curtains. This facility provided pioneering work in the field through the mid-1950s [4]. This facility provided experimental data of discrete sharp edge gusts on aircraft bodies which could be compared to field measurements in aircraft.

Though less common, this style of gust generation and testing is still in use. The University of Maryland has recently conducted similar work in a tow tank facility [15]. An advantage of using water as the working fluid for this method is that similar Reynolds numbers can be achieved at lower model speeds. Models are towed through a tank of mostly quiescent water, except for a section with a transverse jet. This jet of known shape and magnitude serves as the gust. This study found that quasi steady estimates of forces were sufficient far from the gust, but closer to the gust they were inadequate.

One advantage of this type of system is that with the gust being generated in a single stationary location. As a result, it is simpler to create and control. Another advantage of this type of testing is that the gust interacts with the model being investigated in a convective fashion (i.e. convective gust). In other words, the gust moves over the tested body at the speed of the body's forward motion. This is opposed to a global gust, where the velocity of the flow field everywhere around the model is changed at the same time. A convective gust more closely replicates conditions encountered whilst aircraft are flying through the atmosphere.

1.1.2 Change in Model Motion

Another method of imposing unsteadiness on an object is moving the object itself. This can be done by changing the direction and orientation of a moving model, such as in a tow tank, or plunging or impulsively moving a stationary model in an already moving fluid, such as a model in a wind tunnel. The same facility at the University of Maryland mentioned in the previous section has also been used to study this technique of gust creation. Specifically, Perrota and Jones [15] compare the differences between model induced motion and the combined model and fluid motion discussed in the prior section. In this comparison, great care must be taken to accurately model and subtract out the inertial forces from the forces measured on the model in order to obtain the hydrodynamic forces. They found that the simulated motion methods used did not accurately capture the effects seen when towing the model past a stationary transverse jet. They noted their simplified model over-predicted the inertial forces on the wing, and a more rigorous model is needed to accurately

predict these forces.

In a separate, collaborative study between the Air Force Research Laboratory and Illinois Institute of Technology, Granlund et al. [8] studied the gust response both with a stationary model in an oscillating freestream, and an oscillating model in a steady freestream. They showed good agreement in both the lift and drag forces produced for the the thin symmetrical airfoils which were tested in oscillating flow either below or above the stall angles of attack of stall.

Model motion is also being used by Georgia Institute of Technology to investigate the effect of active flow control [1]. Their model employs a two degree-of-freedom system, pitch and plunge, with rapid feedback control to prescribe motion to the tested airfoil. With this method they were able to test methods of gust rejection, significantly reducing upward drift of a model exposed to a sudden upward gust. From these examples it is clear that model motion, when applied correctly, is capable of generating a wide variety of gust shapes and is widely used.

1.1.3 Change in Fluid Motion

This method of generating unsteadiness is the most common and a large number of facilities have been modified, or purpose built to do this. The three main types of gusts generated in this manner include streamwise gusts, transverse gusts and convecting disturbances.

Transverse gusts are often generated by oscillating upstream airfoils. These airfoils deflect the flow from the undisturbed direction, essentially imposing a change in the angle of attack of the model being tested. NASA Langley was again one of the first in the field with their modifications of their Transonic Dynamics Tunnel. A pair of synchronized vanes were installed upstream of the test section in the contraction as pictured in Figure 1.2. These vanes created a sinusoidally oscillating flow in the test section to investigate the response of aircraft models flown on a system of suspension cables [9]. This facility produced many studies on aero-elasticity, notably a verification study comparing wind tunnel measurements of a scaled B-52 aircraft model to flight tests of non dimensional wing bending as a response to gust. This study showed good agreement between wind tunnel tests, flight tests and analytical predictions.

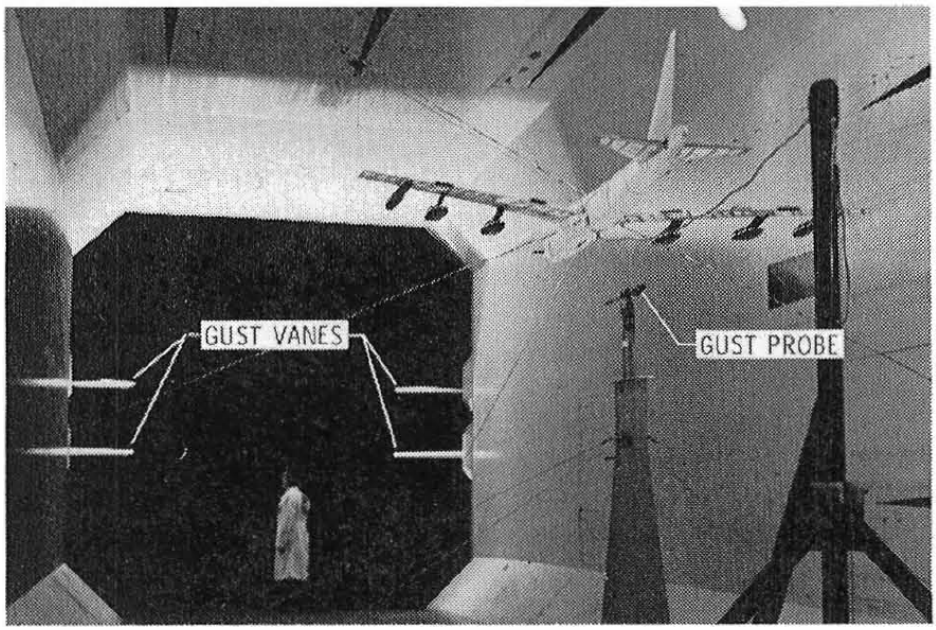

Figure 1.2: The Transonic Dynamics Tunnel at Langely with the gust vanes installed upstream of a scaled B-52 aircraft model [9].

Similar systems have been installed in several other facilities, though the gust generating airfoils tend to span the width of the tunnel and are typically placed at the entrance of the test section. The Delft University of Technology and The Aeromechanical Systems Group in Shrivenham, UK, have both used airfoils at the exit of the wind tunnel contracton into an open test-section wind tunnel[11, 20]. Both have been able to produce reliable sinusoidal variations in the transverse component of velocity in their open test sections. Similar success has also been achieved in wind tunnels with closed test-sections. The University of Bristol, the Politecnico di Milano, and the Beijing University of Aeronautics and Astronautics have all installed a pair of airfoils upstream of their test sections [24, 18, 26]. These facilities have looked into aeroelastic response of structures as well as gust rejection methods. Tang and Dowell at Duke University have made a similar, but unique system, employing rotating slotted cylinders paired with stationary airfoils to create lift to divert the flow [22]. This system was used in the comparison of the theoretical predicted and experimentally measured gust response of high aspect ratio wing sections [23].

Another unique system is the Deterministic Disturbance Generator at Virginia Tech [7]. This

Figure 1.3: The Unsteady facility at Politicnica di Milano. The pair of gust generation vanes are seen to the right of the airfoil being tested[18].

device, located in the contraction of the tunnel, consisted of 10 independently controlled vanes spanning the tunnel. Because of the independent control of the vanes, this system is capable of creating a wide array of gust shapes. They have produced gusts of similar quality to the aforementioned facilities. Research in these facilities includes work with MAVs, aeroelasticity and gust alleviation as transverse gusts are present for vehicles flying through the atmospheric boundary layer.

Streamwise Gusts involve changing the magnitude of the free stream velocity. This is most commonly done with a system of shutters. With the shutters acting as a method of varying pressure loss in the system, the tunnel velocity can be changed without changing the fan power. The shutters allow for significantly faster time response than varying motor power, allowing for rapid changes in the wind tunnel speed.

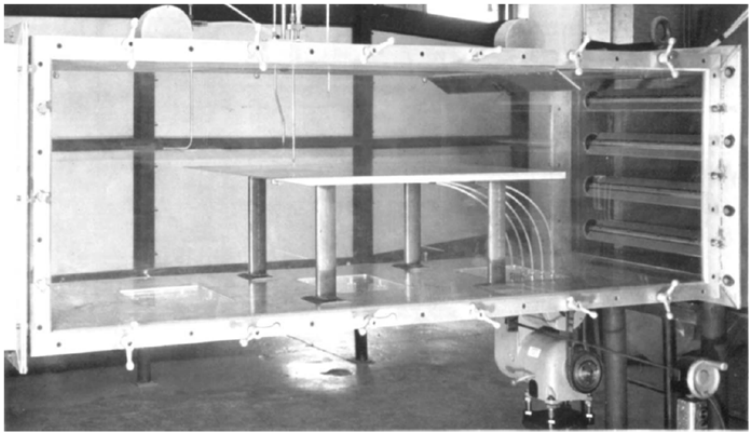

Figure 1.4: The Fejer Unsteady Wind Tunnel at IIT. Louvers are seen on the right, downstream of the test section [13].

The Fejer wind tunnel at the Illinois Institute of Technology was one of the first facilities constructed of this type. This closed-return, closed-test section tunnel included a set of eight blades, in four counter-rotating pairs, located at the exit of the test section shown in figure 1.4. The blade widths were varied to change the portion of the tunnel area which was blocked when the blades were perpendicular to the flow. This tunnel produced early fundamental work such as observations of boundary layer properties in an oscilating flow [13]. The tunnel was recently requalified by Rennie et al. [17] A position controlled servomotor was used to oscillate the vanes based on a $sin^2(\omega t)$ profile which produced near sinusoidal oscillations in the test section speed. This profile compensated for the nonlinearity of the loss coefficient over the louvers as a function of vane angle. Frequencies from .5 - 2 Hz were tested to validate a mathematical model developed for the wind tunnel, which showed good agreement for the cases tested.

A similar facility was created in an open return wind tunnel at Georgia Institute of Technology [16]. In particular, the oscillating free steam was used to to investigate unsteady effects of helicopter blades passing from the side of their rotation into the relative wind to the side against it. Arizona State University also constructed an unsteady wind tunnel [21]. This closed return tunnel, being purpose built for oscillating flows, incorporates a bypass around the test section to keep air flowing through the fan.

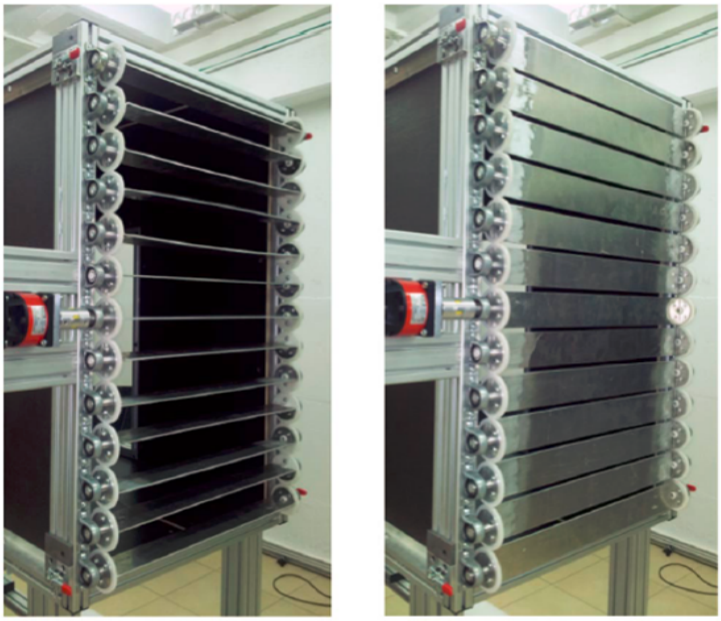

Figure 1.5: The Unsteady facility at the Israel Institute of Technology [6].

Most recently the Israel Institute of Technology modified their open return wind tunnel facility with a set of shutters at the test section exit [6]. Greenblatt [6] describes not only the construction and testing of this tunnel, but also provides a mathematical model predicting the time response of the wind tunnel in unsteady operation. This system consists of 13 symmetrically actuated vanes at the ext of the test section, shown in figure 1.5. The vanes when fully closed block roughly 95% of the exit area, and are capable of statically reducing the test section speed to roughly 20% of the open test section speed. Sinusoidal oscillations of the freestream speed were created using adaptively created ramp up, hold, ramp down, hold profiles in vane angle. These profiles, and resulting test section speed measurements are shown in figure 1.6. Of note is how the profiles are not symmetrical in time for the ramp up and ramp down portions of the position signal. Though not discussed in the paper, this suggests that accelerating and decelerating the flow could have different time responses.

Another method of distorting the flow is creating an upstream disturbance, and allowing the disturbance to advect downstream and interact with the body of interest. In its simpliest form, this

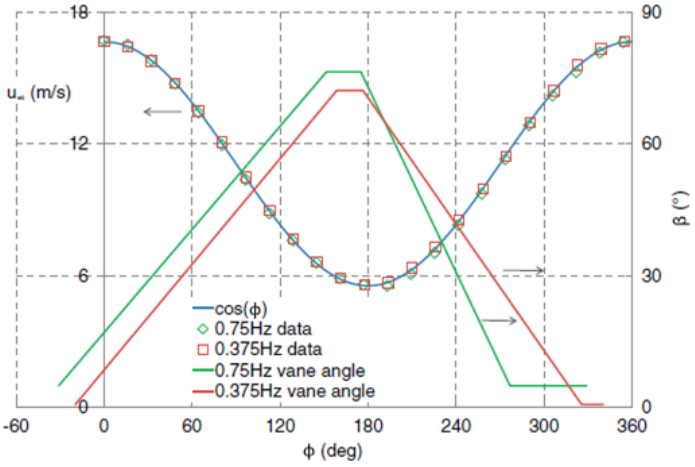

Figure 1.6: Vane angle profiles used to generate sinusoidal freestream speed oscillations at the Israel Institute of Technology Wind Tunnel [6].

can be done with a passive turbulence generating grid [3]. A modification to this system is to make an active grid, or grid with changing properties to excite different scales of turbulence or influence the flow in different regions of the cross section at different times. An active grid for turbulence generation was desigend and built by Mohseni et al. at the University of Colorado Boulder for the purpose of testing MAV response [19]. This grid was compared to turbulence generated from a passive grid, and to atmospheric turbulence. More specific and organized disturbances can also be created. At the Technische Universität Braunschweig an airfoil upstream of the test section is impulsively pitched, creating a transverse vortex, which travels downstream through the test section and interacts with a model[10].

1.2 Method of Interest

Of the discussed methods of gust generation in a wind tunnel environment, a shutter system causing fluctuations in the magnitude of the free stream velocity appears to be the most promising and practical candidate for construction and implementation. Most research that has been done in this area has looked at a sinusoidal oscillating velocity field, and not much work has looked at discrete global variations in the free stream velocity. While several facilities have either implemented

shutter type gust generators either in closed return tunnels or at the test section exit of open return tunnels, there is a limited amount of literature on shutters upstream of the test section. Downstream shutters necessitate a closed-test section so that the pressure change causes a subsequent change in velocity upstream in the test section. Upstream shutters allow for an open or closed test section, giving a wider range of test options.

The objective of this work is to create an upstream shutter system for the existing low-speed wind tunnel facility within the Experimental Aerodynamics Laboratory at the University of Colorado Boulder. This system should be capable of creating impulsive or discrete variations in the magnitude of the test section velocity, imposed globally with a closed test section, or imposed convectively with an open test section.

Chapter 2

System Design

2.1 CU Wind Tunnel Description

This gust generation system was built in the Experimental Aerodynamics Laboratory at the University of Colorado Boulder (CU). This facility includes a low-speed open-return blow-down wind tunnel capable of test section speeds up to 70 m/s which is pictured in Figure 2.1 The wind tunnel was designed and built by Aerolab LLC and is powered by a Twin City Fan BAE-SWSI 600. This is a single wheel, backwards inclined airfoil blower. The blower is powered with a 100 Hp electric motor connected to the blower with a belt drive. The blower outlet is connected to the settling chamber with a flexible rubber coupler. This allows for separation of the blower from the rest of the wind tunnel to reduce transferred vibrations. The diffuser at the entrance of the settling chamber has a 2.5:1 area ratio, expanding from 47.4 in x 67.5 in to 90 in x 90 in. At the exit of the diffuser is a flow straightener consisting of 4 in of aluminum honeycomb. After the flow straightener there are two turbulence reduction screens, with space to install upto two more screens. The contraction has a 9:1 area reduction, going from the 90 in square settling chamber to the 30 in square test section. The test section consists of three removable sections of 30 in x 30 in x 47 in. After the test section is a 2.5:1 area ratio diffuser which discharges into the lab space.

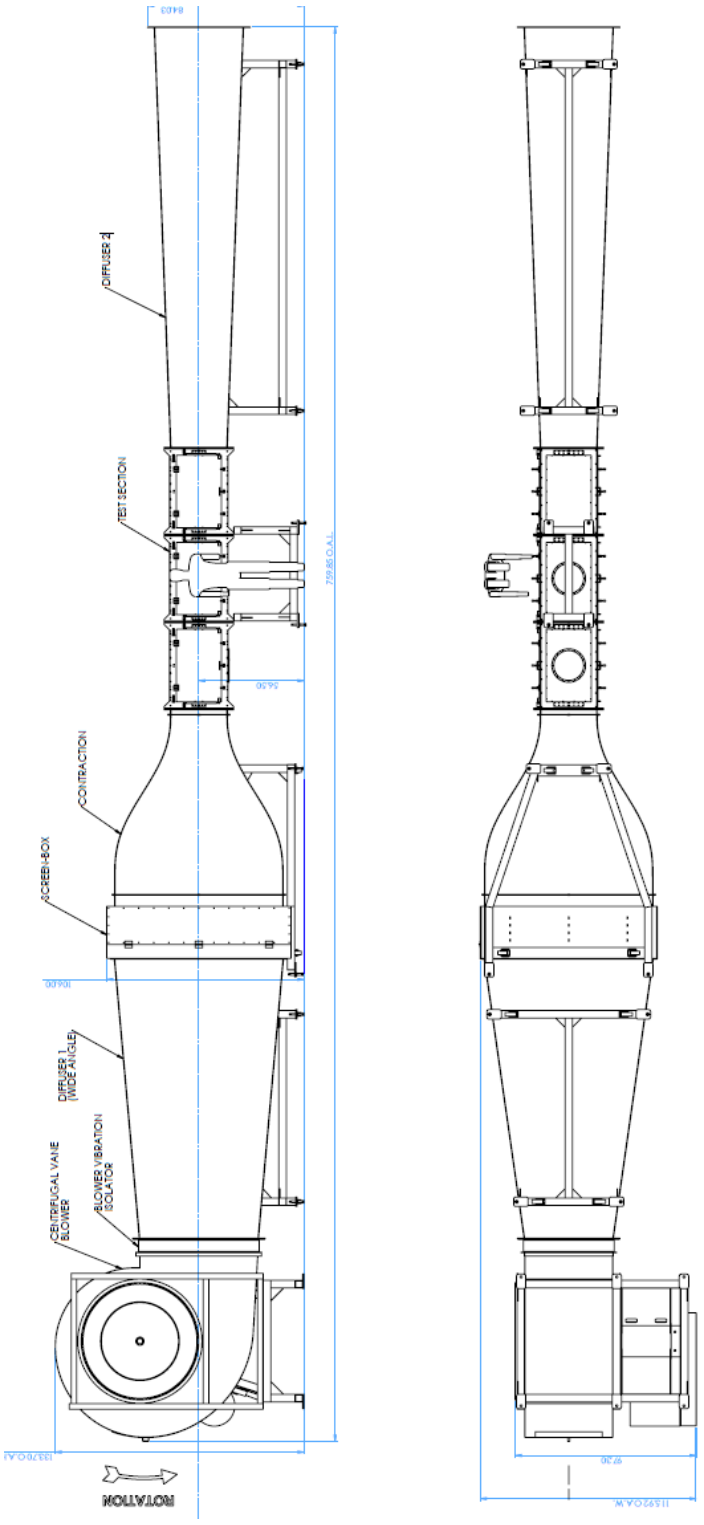

Figure 2.1: The low-speed wind tunnel at the University of Colorado Boulder

2.2 Design Considerations

2.2.1 Generator Type

Many gust generator types were considered in the early design phase. These included pressurized chambers which could be impulsively opened, transverse jets, and controlled pitching of upstream airfoils. These designs considered mainly impulsive transverse gusts. However, after the publication of Greenblatt's paper [6], the opportunity presented itself to further investigate streamwise gusts. Greenblatt's tunnel system, like most of this type, included downstream louvers, which necessitate a closed test section. Our objective was to design a system which could use a closed or open test section. For this reason a design based on a set of upstream louvers was selected.

2.2.2 Generator Location

With the requirement that the louver system be located upstream of the test section, based upon the generator type discussion in the previous section, there were several potential locations in which the system could be installed. The first location considered was in the wind tunnel settling chamber, where the current turbulence reducing screens are installed. Installation of a system here was successfully accomplished in the facility discussed by Charnay et Mathieu [2]. The CU Boulder wind tunnel includes a screen box in the settling chamber, with a recessed area around the outer wall of the tunnel for the addition of extra screens. This could potentially house framing and linkages between airfoil sections, allowing for minimal modification to the wind tunnel itself. After much consideration, this design was abandoned due to several limitations caused by the tight space requirements of housing the system within the screen box. There were also additional concerns related to actuating the large span airfoil vanes at a fast-enough rate to imposed discrete gusts.

The next two locations considered included immediately downstream of the fan, and just upstream of the fan. Immediately downstream of the fan was considered initially because it is still enclosed within the wind tunnel. Despite the fact that this design could be externally constructed as a separated module and easily installed, it would require moving the plenum, test section and

diffuser of the wind tunnel. Moving most of the wind tunnel was impractical, so this location was also abandoned.

The location which was ultimately selected was just upstream of the tunnel inlet. This location provided easy access to the vanes, allowing for simple construction. The system would be similar to an inlet box damper. As this style of damper has been used in industry there is some knowledge of how it affects fan performance and limitations of these devices imposed by fan stall. An additional advantage of this location is that any irregularities in the flow from the generator will have negligible impact on the flow field in the test section, due to the downstream passage of the flow through the fan.

2.2.3 Fan Stall Considerations

When limiting the flow into a fan, one fairly important consideration is stalling the fan. The limited flow rate acts similar to increasing the angle of attack of the fans blades. Once this reaches a certain flow rate, or angle of attack, the fan blade will stall. With a centrifugal fan there are two types of stall which can occur, stall and rotating stall [12].

Rotating stall is a stall specific to centrifugal fans. At low enough flow rates, the fan can no longer maintain the pressure gradient across itself. While most of the cells (passages between fan blades) flow in the normal direction, some of the cells begin to flow in reverse. These reverse flowing cells travel around the fan, causing severe oscillations in pressure at a frequency of two thirds times the rotation rate of the fan itself. This vibration can excite harmonics in the fan or downstream in the wind tunnel, and is capable of causing severe damage.

Both types of stall can be prevented by ensuring that an adequate flow rate is maintained through the fan. One of the goals of testing the system will to be to identify the onset of rotating stall so as to avoid those operating conditions in the future.

2.2.4 Motor Sizing

An estimate of the torque required to operate the system was calculated to select an adequate motor for dynamically operating the system. With gust profiles in mind, there were two important factors in considering the torque on the system. There is the torque imposed by the flow around the apparatus, and the inertia of the system as its rotation rate is changed. The Inertial Torque was fairly straight forward to estimate as the torque on a rotating system, T, is described by the following

$$T = \sum I\ddot{\theta}. \tag{2.1}$$

Where I is the moment of inertia of the system and $\ddot{\theta}$ is the second derivative of the angular position, or angular acceleration, of the system. The torque required to accelerate the system is equal to the sum of the products of the moments of inertia for each of the rotating parts and there respective rotational accelerations. The moment of inertia values for the system were acquired from the SolidWorks model of many of the parts, and from manufacturer info for the motor and gearbox and are displayed Table 2.1.

Table 2.1: Moment of inertia for each system part

Part	Quantity	Moment of Inertia $N * m^2$
Motor	1	.001372
Gearbox	1	.000750
Shaft Coupler	1	.000413
Shaft	20	.00015
Gear	20	.01176
Airfoil	10	.07512
Bearing	20	.000005
Total	-	.99195

Using these values, it was possible to estimate the torque required to accelerate the vanes along certain paths. The accelerations were then estimated using a simple sinusoidal profile with

amplitude, A, at angular speed, ω:

$$\theta = Asin(\omega t). \tag{2.2}$$

From which the second derivative, angular acceleration, can be expressed as the following

$$\ddot{\theta} = -A\omega^2 sin(\omega t). \tag{2.3}$$

The maximum inertial torque can be estimated by multiplying the maximum value of $\ddot{\theta}$ by the system moment of inertia. A 1 Hz sine wave of 90° requires a maximum inertial torque of 30 N $\cdot$ m, before any mechanical losses.

The aerodynamic torque is a less significant part of the total torque on the system. When the flow over the airfoil is attached, about the range of -15° to +15°, there is a torque generated because the center of lift is forward of the point of rotation. Since the NACA 0015 airfoils utilized are symmetric there will be no moment about the aerodynamic center when the flow is attached, so calculating the lift force and moment arm length from the pivot point to the aerodynamic center will provide enough information to give a static torque. Provided that the rotational axis of the vanes is at the half cord point, and the aerodynamics center for a symmetric airfoil is at the quarter cord point, providing a moment arm of $c/4$ and a torque estimate of

$$T_{aero} = \frac{c}{4} qSC_{L_{max}}. \tag{2.4}$$

Note that q is the dynamic pressure and S is the vane planform area and $C_{L_{max}}$ is the maximum lift coefficient for a NACA 0015 profile.

A test section speed outside of the anticipated operating range of the system was selected to calculate the maximum holding torque. Specifically, a test section speed of $U = 55$ m/s corresponds to a chord-length based Reynolds number of approximately $Re = 1 \cdot 10^5$ for the airfoil vanes at the wind tunnel inlet. For a NACA 0015 airfoil at this Reynolds number the max T_{aero} occurs around $\alpha = 12.75°$. The maximum T_{aero} is 0.634 Nm per blade, or 6.34 Nm total for the system of 10 blades. While this is significant, it is much lower than the inertial torque requirements estimated for dynamically accelerating the system. Also note that after stall the airfoil is similar to a flat plate.

With a pure flat plate assumption, there is no torque around the half cord point, so aerodynamic torque in the fully stalled region was neglected for motor sizing estimates.

Knowing that a peak torque 30 Nm and the maximum holding torque of 6.5 Nm is required, it is possible to select a motor which will meet the requirements of the system. At first single motor systems were considered, however these motors were excessively large and quite expensive. This lead to the consideration of motors paired with gearboxes. The motor which was ultimately selected was the Teknic M3441 with a CGI Motion 034PLX 3:1 gearbox. This motor has a continuous torque rating of 3.32 Nm and a peak torque rating of 14.14 Nm. When geared back with the 3:1 gearbox it has a continuous torque rating of 9.96 Nm, and a peak torque rating of 42.42 Nm. These exceed the minimum estimated torque requirements put forth as selection criteria earlier in this section.

Note that this motor was selected for several reasons. The motor met the requirements put forward and was within the budget. The Experimental Aerodynamics Lab already operates two Teknic motors, including one M3441, so there was the added benefit of consistency. This consistency also drove the selection of the encoder resolution. The aim was to have sub-0.1° resolution, necessitating and encoder with over 4000 counts per revolution. Since the M3441 motor already being used in the lab had a 16000 count per revolution encoder, it was decided to purchase an identical motor, allowing one to potentially serve as a backup for the other on future projects. This meant that when geared, the system had an encoder equivalent to 48000 counts per revolution, or resolution of 0.0076° providing excellent resolution; even if noise interference causes missed counts.

2.3 Final Design

The final design incorporated 10 NACA 0015 airfoil vanes installed at the wind tunnel inlet in a box style damper system as pictured in Figure 2.2. These 10 vanes allowed for 85% of the projected area to be blocked when the system was fully closed. The vanes were mounted to two spur gears, one on top, one on bottom. The gears had a pitch diameter of 6.25 in allowing for a 0.25 in passage between each vane when closed. The gears caused the airfoils to counter-rotate, meaning that the flow exiting the generator was left-right and top bottom symmetric. While the

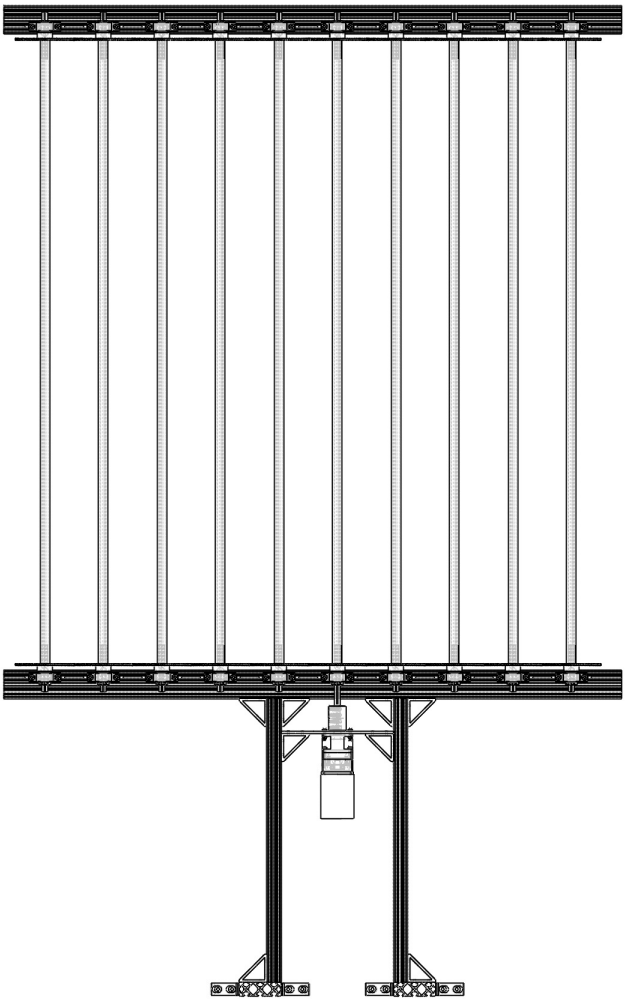

Figure 2.2: Front view of the gust generator

flow is not uniform, flow directed significantly to one side of a centrifugal fan inlet results in a drop in efficiency [25]. Above and below the gears, low profile mounted ball bearings allowed for smooth rotation of the vanes. A close-up view of the mounted gear and bearing assembly is presented in Figure 2.3.

The NACA 0015 vanes were mounted to 1/2 in shafts which protruded from the top and bottom of each section. Two plugs machined from aluminum matched the inside profile of the airfoils and hold the shaft at the half cord point. A keyway in both the shaft and plug allowed

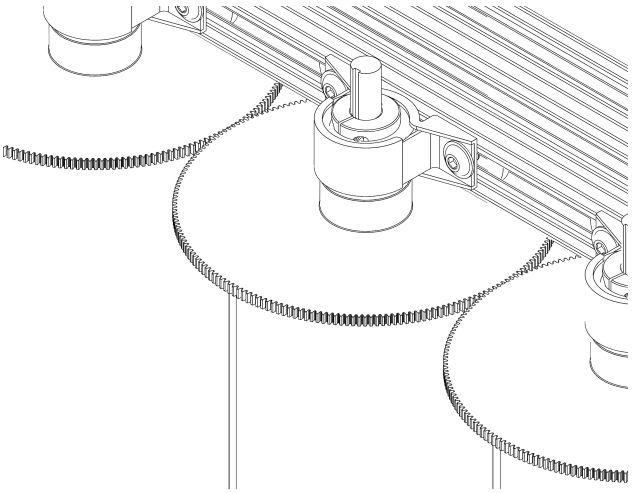

Figure 2.3: An isometric view showing the gears on top of the airfoils, the bearings, and shafts.

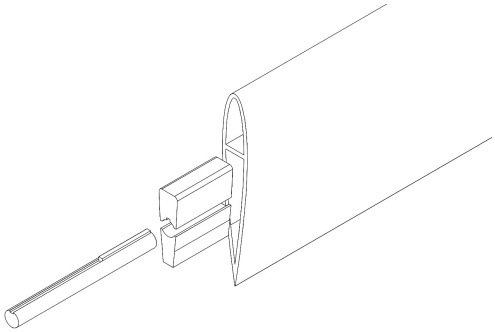

Figure 2.4: An exploded view of the airfoil vane-shaft assembly.

for transmission of torque between the airfoil and shaft. Figure 2.4 presents an exploded view of this shaft-vane assembly for reference. Set screws on the gear, bearing and a clamp-on collar hold the shaft in place. Since the airfoil sits between two bearings, one top and one bottom, a tight fit ensures no vertical movement of the airfoil throughout its operation.

The motor, which was used to dynamically actuate the damper system, is mounted in a frame directly below the inlet of the wind tunnel as pictured in Figure 2.5. This takes advantage of a lower member of the wind tunnel structure, allowing for a very stiff frame. The horizontal and vertical rails of 80/20 allow the motor to be aligned to the central airfoil vane before being locked in place. Attached directly to the motor is the 3:1 planetary gearbox, while a custom-bored rigid,

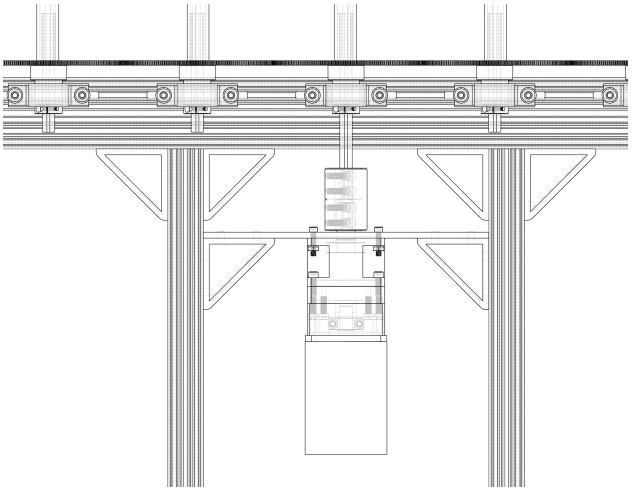

Figure 2.5: A detail view of the mounted motor.

step-down shaft coupler connects the motor to the shaft of the middle airfoil vane.

2.3.1 Motor Control

The motor is controlled by the Copley Controls Accelnet MicroPanel servo drive. A custom National Instruments Labview program was written to send a continuous position signal to the servo drive. The servo drive receives encoder feedback from the motor. As discussed in the previous section the encoder has an equivalent of 48000 counts per revolution, providing excellent resolution. Using the CME2 software provided by Copley Controls with the drive, the system was tuned for the motor and shutter system. Speciffically, a position mode control algorithm was utilized which includes proportional position gain, velocity feed forward gain, acceleration feed forward gain, and a total gains multiplier. This was part of a larger structure, which fed into a velocity control loop, and finally into a current control loop. This general controller architecture is pictured in Figure 2.6, taken from CME2, with an additional detail of the position loop included in Figure 2.7. Once installed in the system the motor was tuned manually to minimize chatter while holding positions as well as position following error. Optimum values found for this application, which were used during testing are shown in table 2.2

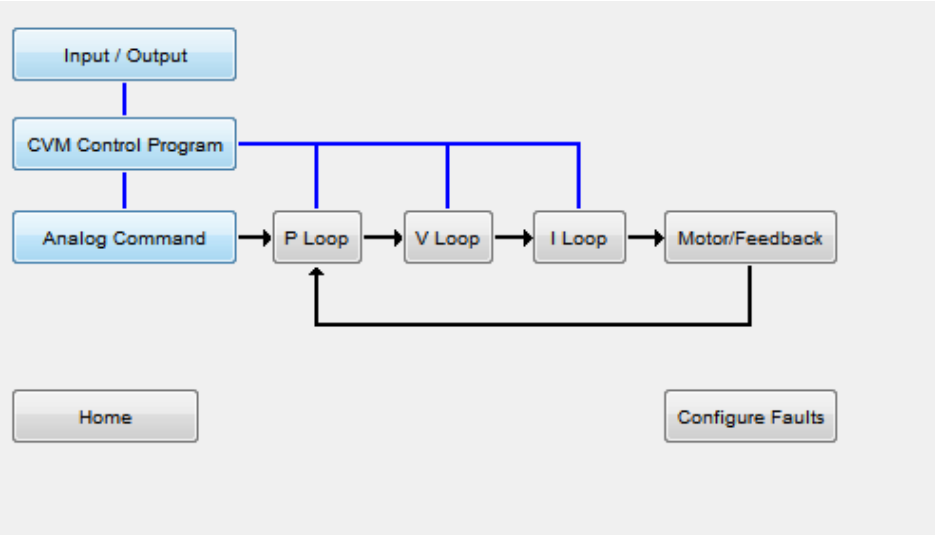

Figure 2.6: Position mode motor control architecture taken from Copley Controls CME2.

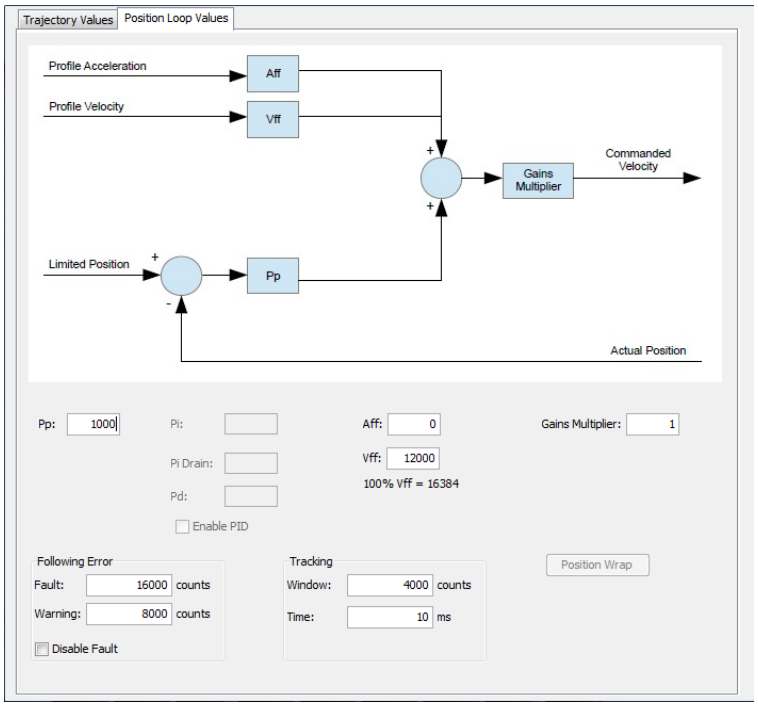

Figure 2.7: Detailed schematic of the position loop within the position mode control architecture from CME2.

Table 2.2: Motor Controller Settings

Parameter	Value
Position Proportional Gain	7500
Velocity Feed Forward	16384
Acceleration Feed Forward	1000
Velocity Proportional Gain	700
Velocity Integral Gain	50
Velocity Integral Drain	0
Current Proportional Gain	236
Current Integral Gain	38
Drive Output	Maximum Smoothness

Chapter 3

Experimental Setup

3.1 Theoretical Model

A mathematical model relating the unsteady wind tunnel performance to the wind tunnel's mean operating conditions and variable exit area was developed and presented by Greenblatt [6]; for a sinusoidally oscillating flow. This section presents that mathematical model, but modified for the CU Boulder wind tunnel facility. The objective is to arrive at a reduced order mathematical model which can help predict the performance of the wind tunnel system. The main modifications include the inclusion of a diffuser at the wind tunnel exit, and accounting for the different location of the louver system.

The first assumption made is that the fluid within the wind tunnel is incompressible. The wind tunnel has an operating range of $U = 0 - 70$ m/s, or $M = 0 - 0.2$, this falls within the incompressible region of air flow ($M = 0 - 0.3$). This allows for the use of the mechanical energy equation along a streamline, or the Unsteady Bernoulli equation, as a starting point:

$$\frac{\partial u}{\partial t} ds + \frac{1}{2}(1 + k_1) d(u^2) + \frac{dP}{\rho} = 0. \tag{3.1}$$

The blower pressure, P_b, can be decomposed into the mean and fluctuating components

$$P_b = \bar{P}_b + \tilde{P}_b \tag{3.2}$$

where

$$\bar{P}_b = \int_0^T P_b(t) dt. \tag{3.3}$$

The volumetric flowrate, Q, can be decomposed in the same way

$$Q = \bar{q} + \tilde{q} \tag{3.4}$$

where

$$\bar{q} = \int_0^T Q(t)dt. \tag{3.5}$$

Also note that at any point in time, the volumetric flow rate is the same at all points within the tunnel due to the incompressible flow assumption.

$$Q = A_b U_b = A_c U_c = A_\infty U_\infty = A_e U_e = A_a U_a \tag{3.6}$$

The velocity is also broken down in a similar way, however it is directly dependent on the cross sectional area of the tunnel and will thus vary throughout the wind tunnel circuit. The velocity through out the lengths of the plenum and test section are assumed to be constant due to their constant cross sectional area and the assumption of inviscid flow. In contrast, the wide angle diffuser, contraction and downstream diffuser all have areas dependent on position, so velocity is also a function of position (s) in these sections. Note that the test-section velocity is defined as $u_\infty(t)$ while the contraction velocity is defined as $u_c(t,s)$. Furthermore, subscripts $_b$, $_e$, and $_a$ are used to represent the conditions at the blower, test-section exit, and wind tunnel exit at atmospheric conditions, respectively.

$$u_\infty(t) = \bar{u_\infty} + \tilde{u_\infty}(t) \tag{3.7}$$

$$\bar{u_\infty} = \int_0^T u_\infty(t)dt \tag{3.8}$$

$$u_c(t,s) = \bar{u_c} + \tilde{u_c}(t) \tag{3.9}$$

$$\bar{u_c}(s) = \int_0^T u_c(t,s)dt \tag{3.10}$$

These decompositions can then be substituted into Equation 3.1. Multiplying through by density, and integrating along a streamline from the blower to the wind tunnel exit (i.e. atmospheric

conditions) gives the following result:

$$\rho \int_b^a \frac{\partial \tilde{u}(s,t)}{\partial t} ds + \frac{1}{2}\rho(1+k_1)[\bar{(u_a)}^2 + 2\bar{u_a}\tilde{u_a} + \tilde{u_a}^2] + [P_a - [\bar{P_b} + \tilde{P_b}]] = 0. \tag{3.11}$$

Time-averaging Equation 3.11 provides

$$\frac{1}{2}\rho(1+k_1)[\bar{u_a}^2 + \bar{\tilde{u_a}^2}] + [P_a - \bar{P_b}] = 0. \tag{3.12}$$

Subtracting the time-averaged result, Equation 3.12, from the general form, Equation 3.11 gives the following unsteady result:

$$\rho \int_b^a \frac{\partial \tilde{u}(s,t)}{\partial t} ds + \frac{1}{2}\rho(1+k_1)(\frac{A_a}{A_\infty})^2[2\bar{u_\infty}\tilde{u_\infty} + [\tilde{u_\infty}^2 - \bar{\tilde{u_\infty}^2}]] = \tilde{P_b}. \tag{3.13}$$

Equation 3.13 relates the fluctuations of the wind tunnel velocity to the fluctuations in the total blower pressure. We can then define the velocity ratio $\epsilon_\infty(t) = \frac{u_\infty(t)}{\bar{u_\infty}}$ and substitute it into Equation 3.13, which produces:

$$\rho \int_b^a \frac{\partial \tilde{u}(s,t)}{\partial t} ds + \frac{1}{2}\rho(1+k_1)\bar{u_\infty}^2(\frac{A_a}{A_\infty})^2[2\epsilon_\infty(t) + [\epsilon_\infty(t)^2 - \bar{\epsilon_\infty}(t)^2]] = \tilde{P_b}. \tag{3.14}$$

For a discrete pulse or finite ramp up and down, over a sufficiently long time domain the mean of the fluctuating component will be near zero, so $\bar{\epsilon_\infty}(t)^2 \approx 0$ and can be dropped from Equation 3.14.

Now as a result of the incompressible flow assumption, the flows speed at any two points in the tunnel can be related by the ratio of their areas. Using this it is possible to define the flow through each section of the wind tunnel based on the test section speed.

$$\widetilde{u}(s,t) = \begin{cases} 0 & b \le x \le c \\ \frac{A_\infty}{A_c(s)}\widetilde{u_\infty}(t) & c \le x \le t \\ \widetilde{u_\infty}(t) & t \le x \le e \\ \frac{A_\infty}{A_d(s)}\widetilde{u_\infty}(t) & e \le x \le a \end{cases} \tag{3.15}$$

This form can be used to evaluate the integral term of Equation 3.14 which can be done in the following fashion:

$$\int_b^a \frac{\partial \tilde{u}(s,t)}{\partial t} ds = \frac{\partial \widetilde{u_\infty}}{\partial t} \int_b^a \frac{A_\infty}{A(s)} ds = \frac{\partial \widetilde{u_\infty}}{\partial t} L_{eq}. \tag{3.16}$$

Where L_{eq} is an equivalent length which results from the integration of the section area ratio along a streamline through the entire wind tunnel circuit. This can be substituted into the first term of Equation 3.14 and the result can be divided by $\frac{1}{2}\rho(1+k_1)\frac{A_\infty^2}{A_a^2}\bar{u_\infty}^2$ which gives the following:

$$\frac{L_{eq}A_a^2}{\frac{1}{2}(1+k_1)A_\infty^2\bar{u_\infty}}\epsilon'_\infty + 2\epsilon_\infty + \epsilon_\infty^2 = \frac{\tilde{P}_b}{\frac{1}{2}(1+k_1)\rho\bar{u_e}^2}. \tag{3.17}$$

Which, if assuming a negligible tunnel loss coefficient k_1 the equation can be simplified to:

$$\tau\epsilon'_\infty + \epsilon_\infty^2 + 2\epsilon_\infty = g(t) \tag{3.18}$$

where

$$\tau = \frac{L_{eq}A_a^2}{\frac{1}{2}A_\infty^2\bar{u_\infty}} \tag{3.19}$$

and

$$g(t) = \frac{\tilde{P}_b}{\frac{1}{2}\rho\bar{u_a}^2}. \tag{3.20}$$

Note that τ is equivalent to a time constant, and $g(t)$ is a non-dimensional forcing function based on the fluctuating component of the total blower pressure normalized by the mean exit dynamic pressure.

There are several main conclusions that can be drawn from this mathematical model. First, when comparing to the analysis done by Greenblatt [6], is that when incompressibility is assumed, the end results take the same form regardless of whether the vanes are located at the exit or inlet of the wind tunnel. The time constant's area terms, however, for this case are based off of the constant area of the exit A_a as opposed to a mean of a fluctuating exit area $\bar{A}_e$ used by Greenblatt. The main differences come with the inclusion of the diffuser, altering the equivalent lengths of the wind tunnel system.

This provides a point of comparison for comparing the experimental results to the model predictions. This form when compared to experimental results severely over predicts the time response of the system, so a form of this result was reduced down to a first order linear equation with experimentally determined constants. ϵ_∞^2 can not simply be ignored to reduce equation 3.18 to a first order linear equation because this term ensures the predicted velocity approaches zero as

blower pressure approaches zero(i.e $\epsilon_\infty \to -1$ as $g(t) \to -1$ is a quasi-steady case.) What can be taken away from these equations is the form of the time constants. The time constant is inversely proportional to mean test section speed. The time constant is also dependent on the equivalent length of the wind tunnel. With this in mind, a first order approximation of the system would take the following form:

$$\tau_1 \epsilon'_\infty + \epsilon_\infty = f(t) \tag{3.21}$$

where

$$\tau_1 = c\frac{L_{eq}}{\bar{u_\infty}}, \tag{3.22}$$

c is an empirically determined constant,and L_{eq} is an equivalent length. $f(t)$ is a forcing function based on the normalized velocity fluctuation. This is form was used to quantitatively estimate the time constants of the wind tunnel system in Section 4.3.

3.2 Experimental Setup

The gust generation system design was in Chapter 2, Figure 3.1 presents a photograph of the final system installed at the inlet of the CU Boulder Low Speed research Wind Tunnel.

Within the wind tunnel test section, three constant-temperature anemometers (i.e. hotwires) were used to measure the unsteady velocity. Two hotwires were positioned at the inlet of the test section. These two signals can be compared to verify uniformity across the test section. These hotwires were mounted to the floor of the test section and were elevated 7 in, well outside of any predicted boundary layer height. The third hotwire was mounted to a traverse system at the rear of the test section. This signal can be compared to the signals from the other two hotwires to observe the speed at which disturbances advect through the wind tunnel test section. Figure 3.4 presents a schematic layout of these wires while Figures 3.5 and 3.6 present photographs of the final test configuration.

Figure 3.1: Gust generator system installed on the inlet of the CU Boulder low-speed research wind tunnel.

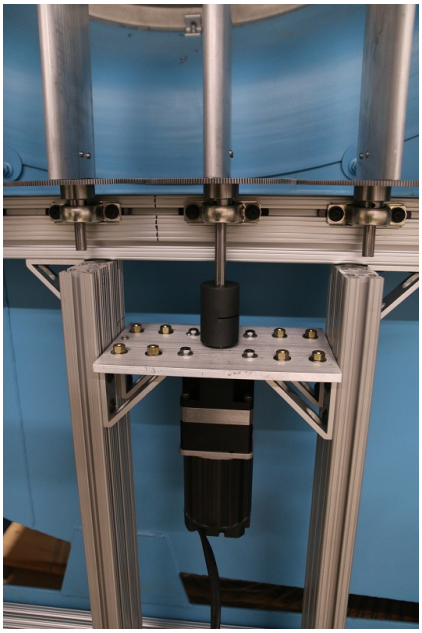

Figure 3.2: Close up of the gust generator motor mounting assembly.

For all experiments the system was controlled by a single LabView program. This program controlled the blower speed of the wind tunnel and read back data from sensors installed in the wind tunnel which measured temperature, humidity, static ring differential pressure. The program

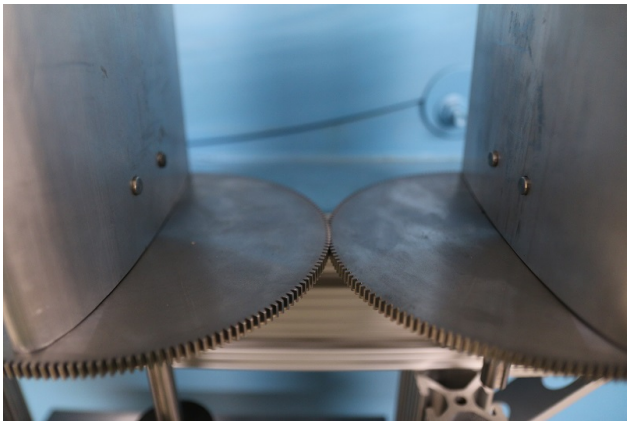

Figure 3.3: Close-up of the gust generator gears and airfoil vane connection.

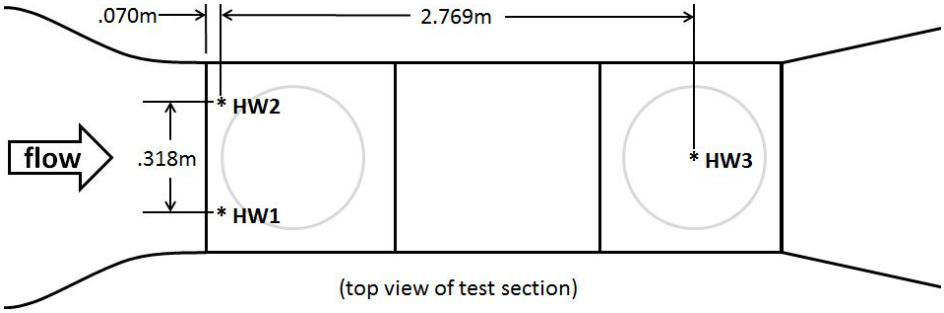

Figure 3.4: Schematic detailing the layout of the CTA hotwires within the wind tunnel test section.

Figure 3.5: Photograph of the upstream CTA hotwires (hW1, hW2) installed in the wind tunnel test section.

created a vane angle profile based on user input and converted it to an analog voltage signal. This analog voltage was the position input for the motor, with the voltage magnitude controlling angular position. When collecting data the program stored the analog voltage written to the motor, encoder

Figure 3.6: Photograph of the downstream CTA hotwire (hW3) installed in the wind tunnel test section.

position, data from all three hotwires, as well as the data from the aforementioned sensors.

3.3 Ensemble Averaging

For the analysis of the data, ensemble averages were considered. To gain an understanding of how the unsteady data sets converge to a mean, two large data sets were collected for a 1 s 90° pulse. 200 pulses were taken at speeds of 10 and 20 m/s, as this was a common speed for tests. The ensemble averages for 1 to 200 ensembles were each subtracted from the total ensemble average of 200 pulses. The root mean square of this deviation from the mean profile was taken and is presented in Figure 3.7.

From this analysis the first 20 ensembles show an order of magnitude reduction in the error. The data then plateaus, and the next order of magnitude reduction of the error requires around 180 ensembles. This was taken as justification to continue using 20 ensembles as the statistical standard for the current study.

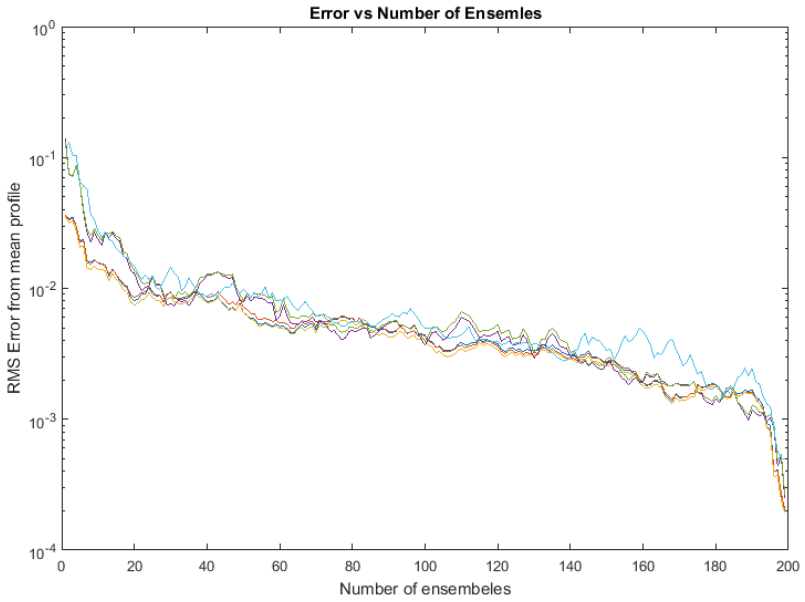

Figure 3.7: Convergence of ensemble averages to mean profile.

Chapter 4

Results and Discussion

4.1 Steady Performance

The first set of tests completed were static tests. The objective of these tests was to qualify the static or steady performance of the system. The data of this test was used to create a function for blower pressure in terms of blower speed and vane angle. This test also served to observe any hysteresis or asymmetries in the system by opening and closing the vanes in both directions. Conditions which could create rotating fan stall were also noted.

For the static tests, the vanes were commanded to hold a single position while the measurements were collected. Addtionally, after moving to a new position a 10 s time delay was utilized before data was taken to allow any transient effects on test section of velocity to settle out. Hotwire and Pitot-static measurements were taken for 10 s at a sample rate of 1 kHz. Measurements were taken at blade positions from $\theta^\circ = 0$ to 90° in increments of $\Delta\theta = 10^\circ$, and back from $\theta = 85^\circ$ to 5°. This was then repeated in the opposite direction (i.e. $\theta = 0^\circ$ to -90° and back from $\theta = -85^\circ$ to -5°) to observe the symmetry of the system. These tests were performed at six motor (fan) speeds $n = 160$, 300, 435, 565, 700, and 835 RPM which roughly correspond to open test section wind speeds of $U_\infty = 5$, 10, 15, 20, 25 and 30 m/s, respectivly.

From the data in Figure 4.1 is clear that the reduction of test section velocity is directly dependent on the blower speed, and the data is not symmetrical with the gust generator vane angle. To better asses these trends the data normalized by the open test section speed for each set motor speed and is replotted in Figure 4.2. When normalized by the full-open speed (i.e. $U_\infty|_{\theta=0^\circ}$),

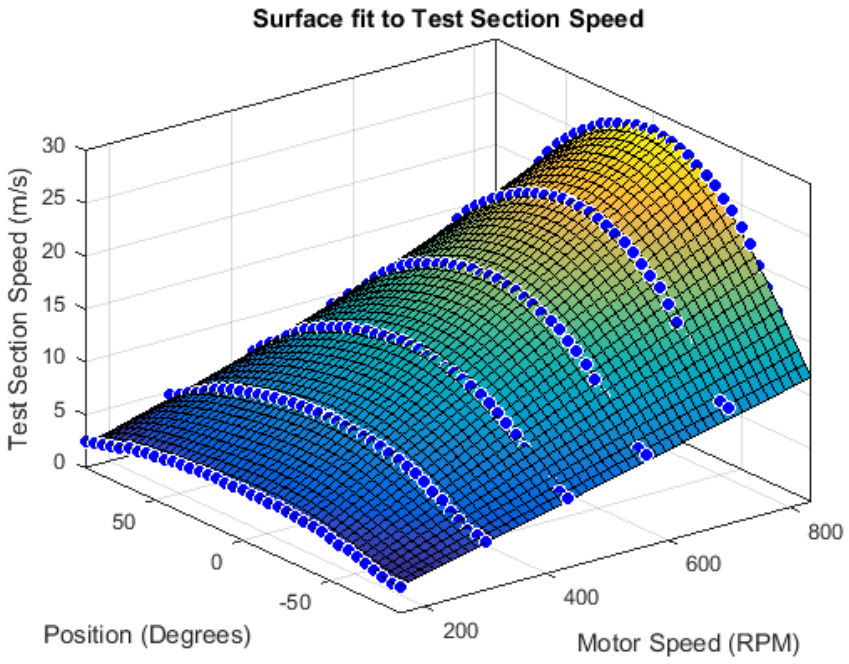

Figure 4.1: Velocity distribution surfaces versus the motor speed and vane angle position for the steady (static) closure of the gust generator vanes.

the data appears to collapse together showing similar reductions in velocity throughout the tested range. There is however a slight dependence on open test section speeds, with higher initial speeds showing a greater overall reduction.

The asymmetry observed in both Figures 4.1 and 4.2 with vane angle is due in part to the effect of the outside vanes. Specifically, there is a gap between the outermost vanes and the edge of the fan-inlet frame. During the different phases of rotation the minimum distance between the outer vane and the corner of the frame, the distance which contributes to the open area of the inlet, is determined by either the position of the leading edge, trailing edge or a point along the wing This difference in geometry means that that the area is reduced along two different profiles leading to asymmetries in the blocked area with respect to the vane angle. If the asymmetry in flow reduction is solely due to these different profiles, plotting the normalized velocity versus inlet area should show the data collapse. Figure 4.3 presents the static normalized velocity data versus the normalized inlet area, accounting for these differences between between the positive and negative

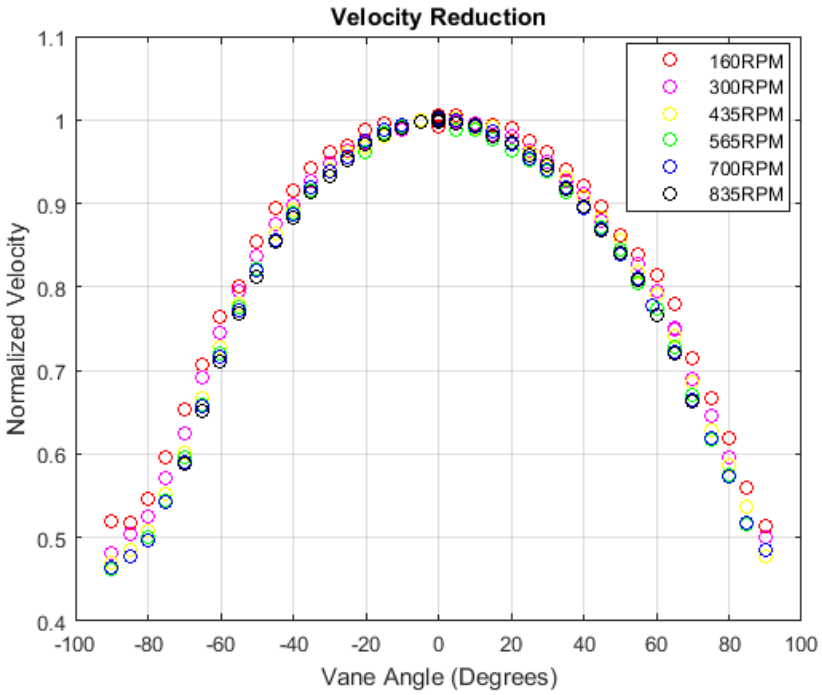

Figure 4.2: Normalized velocity distribution vane angle position for the steady (static) closure of the gust generator vanes.

vane positions. Once properly accounted for, the data collapses down to a single nonlinear curve with respect to the open area through vane system. This shows that the overall reduction in test section velocity is a function of inlet area. Furthermore, simple modifications to the system could easily improve the symmetry in the data with respect to the vane closer angle, θ, allowing for for a further range of vane angle profiles to be created.

Throughout the static qualification, attention was paid to the blower for signs of fan stall. No indications of rotating stall of fan stall were observed. The test was cut short due to vibrations present in the vanes at angles greater than $\theta = 70°$ and open test section speeds of $U_\infty \geq 30$ m/s. This gives a working range for the system of $U_\infty = 0$ to 25 m/s test section speeds for $\theta = 0°$ to 90° closures, and limited closures up to $U_\infty = 30$ m/s open test section speed.

As an additional check of functionality, the wind tunnel was run through its entire range of speeds with the gust generator installed. The two tests were run: (1) once with the mechanical wing clamp installed and the motor disengaged, and (2) once with the mechanical wing clamp

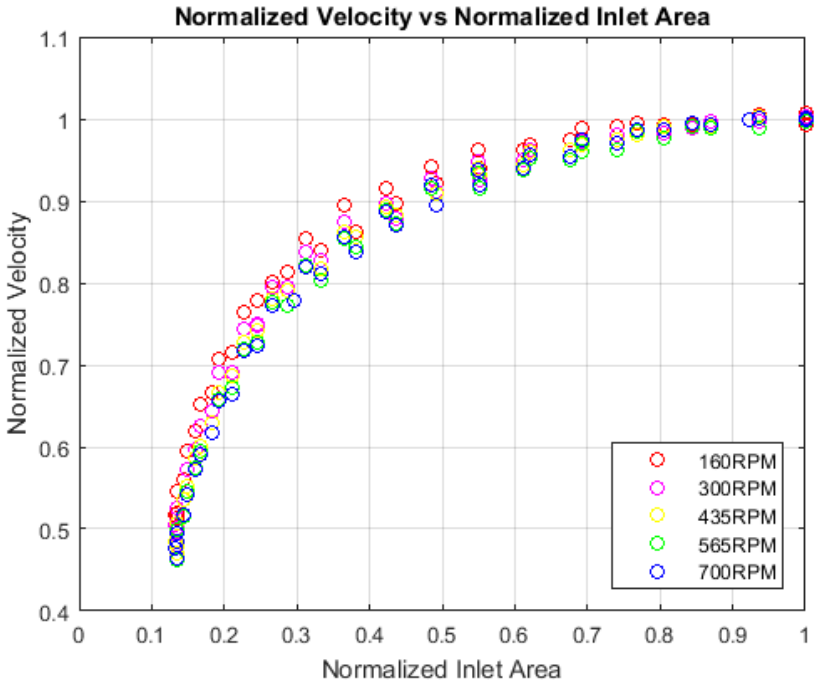

Figure 4.3: Normalized static velocity distribution versus the normalized inlet area through the vane system.

removed and the motor statically holding a vane angle of $\theta = 0°$. In both configurations the tunnel was run to its maximum speed, $n = 1800$ RPM or roughly $U_\infty = 70$ m/s test section speed. In both cases, minimal vibrations were observed suggesting that the installation of the gust generator system (even when not in use) has not compromised the functional capabilities of the wind tunnel.

4.2 Unsteady Performance

Verification of the unsteady performance of the gust generator system incorporated tests with three different time-dependent motion profiles, including: (1) a periodic sine wave, (2) a discrete $1 - Cosine$ impulse, and (3) a linear ramp. These waveforms were selected to fully investigate the transient effects of the system and the wind tunnel as a whole. The following sub-sections discuss the tunnel response to each of these profiles.

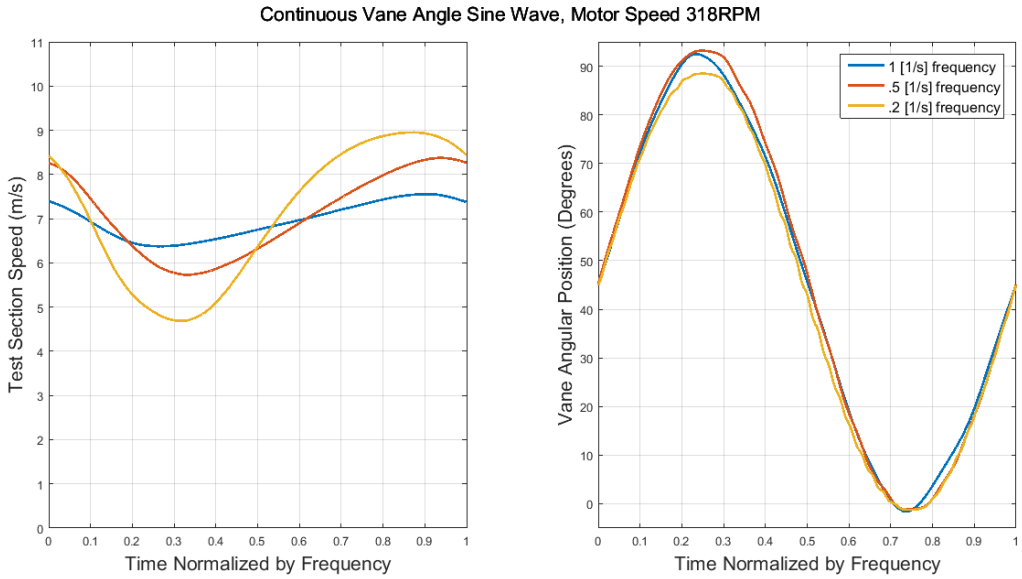

Figure 4.4: Wind tunnel test section velocity response to a periodic sinusoidal vane angle prescription at three normalized frequencies and a motor speed of $n = 318$ RPM.

4.2.1 Periodic Profiles

One of the most commonly investigated profiles for a longitudinally unsteady wind tunnel is sinusoidal oscillations of the free stream velocity. Attempting to create a sinusoidal oscillation would give a point of comparison to established work, and provide further understanding into the dynamics of the tunnel system.

First, and most simply a continuous sine wave of the vane's angular position was commanded. The amplitude of the oscillation was $A = 45°$,and was offset $\bar{\theta} = 45°$ such that the peaks of the sine wave were $\theta_{min} = 0°$ and $\theta_{max} = 90°$. These sinusoidal profiles were tested for periods of $T = 1$ s, 2 s, and 5 s at motor speeds of $n = 318$ RPM and 600 RPM which correspond to $U_\infty|_{\theta=0°} = 10$ m/s and 20 m/s respectively. Twenty ensembles were taken for each case, and averaged together the results of which are presented in Figures 4.4 and 4.5 for $n = 318$ RPM and 600 RPM, respectively.

A clear asymmetry in the test section velocity can be observed between opening and closing of the vanes for all of the dynamic profiles tested. This consistent difference in accelerative and

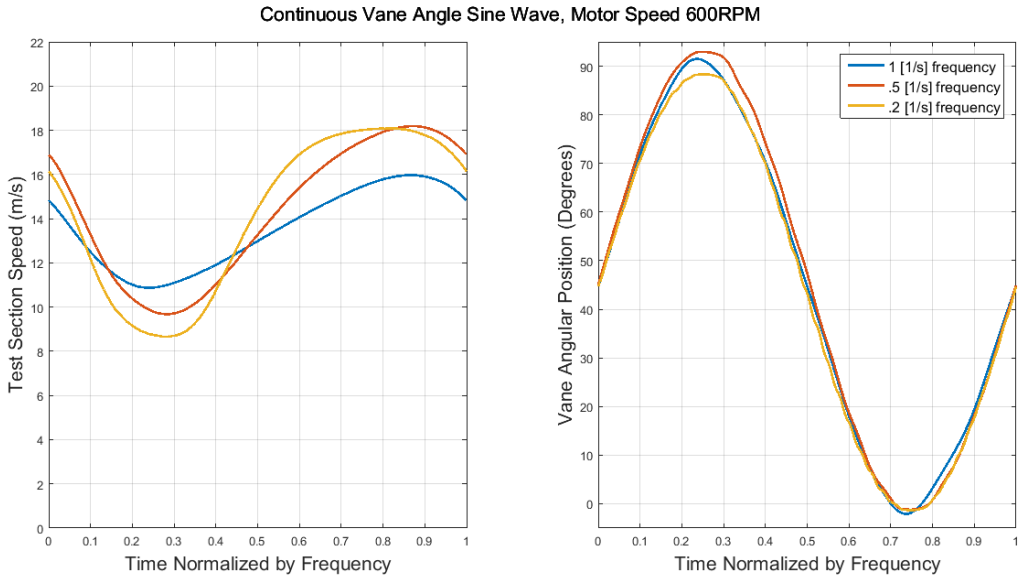

Figure 4.5: Wind tunnel test section velocity response to a periodic sinusoidal vane angle prescription at three normalized frequencies and a motor speed of $n = 600$ RPM.

decelrative time constants is discussed further in Section 4.2.2 This asymmetry is most noticeable for case where the oscillation period is $T = 1$ s, where 60% to 70% of the oscillation period is spent with the flow accelerating. This asymmetry becomes less significant as the oscillation period is increased to both $T = 2$ s and reduced even further as the period approaches $T = 5$ s. With this understood, it is clear that any attempt at sinusoidally varying the free stream velocity will have to relate the frequency to the ratio of time spent opening to closing.

A first attempt at creating a truly sinusoidal oscillation in the test-section velocity achieved reasonable success and is presented in Figure 4.6 for both two and five second periods sine wave at a motor speed of $T = 318$. More specifically, the five second period sine wave had a symmetrical vane angle command along a profile generated by relating the vane angle to the test section velocity and fitting this to a sine wave. The profile for the $T = 2$ s period sine wave was generated in the same way, but the decelerative portion of the sine wave was 0.75 seconds and the accelerative portion of the sine wave was 1.25 seconds.

A reasonable amount of success was also achieved for $T = 600$ RPM the results of which

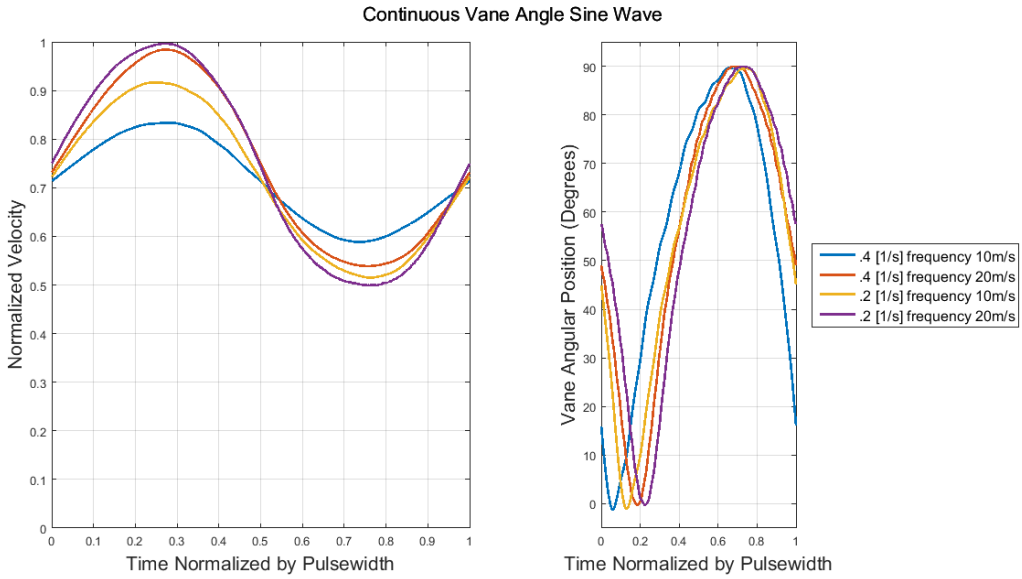

Figure 4.6: Wind tunnel test section's 'quasi-sinusoidal' velocity response to a modified periodic vane angle prescription at three normalized frequencies and a motor speed of $n = 318$ RPM.

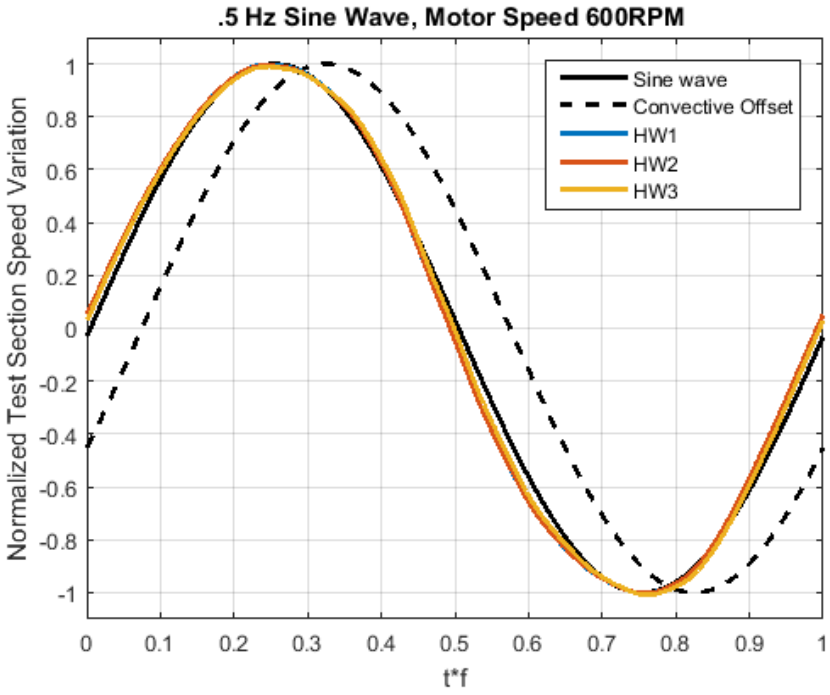

Figure 4.7: Wind tunnel test section's 'quasi-sinusoidal' velocity response to a modified periodic vane angle prescription at a frequency of $f = 0.5$ Hz and a motor speed of $n = 600$ RPM.

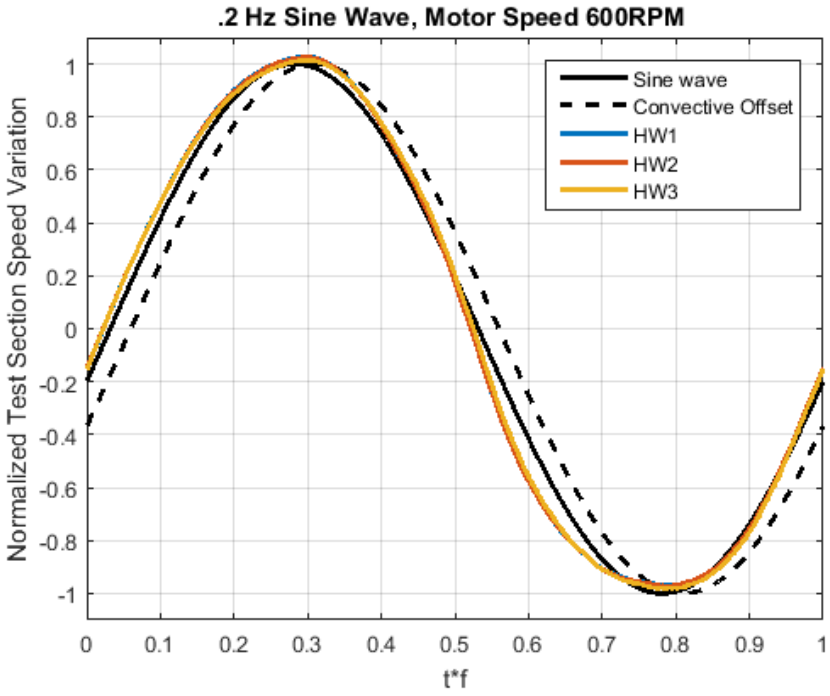

Figure 4.8: Wind tunnel test section's 'quasi-sinusoidal' velocity response to a modified periodic vane angle prescription at a frequency of $f = 0.2$ Hz and a motor speed of $n = 600$ RPM.

are plotted in Figures 4.7 and 4.8. For comparison a sine wave was plotted with the amplitude and phase matched to the the velocity fluctuations. What can be seen here is that the asymmetry seen in the previous case, vane angle sine wave, is no longer present. The asymmetric input of the two second period sine wave ($f = 0.5$ Hz) was enough to counter any asymmetries in the tunnel response between opening and closing the vanes. The five second period sine wave had sufficiently approached steady state to the point where the asymmetries were no longer significant enough to cause a significant difference in the time for the velocity to accelerate and decelerate. This shows similarities to the the profiles generated by Greenblatt [6] in that the closing of the vanes is faster than the opening to achieve a sinusoidal oscillation. Also plotted in each of these figures is a sine wave offset from the first sine wave by a phase equivalent to a convective lag between the front and rear hotwires. This suggests that the disturbances are advecting through the test section significantly faster than the mean test section speed, which is discussed in more detail in Section 4.3.

4.2.2 Impulses

Moving from the continuous periodic profiles discussed in the previous section the remainder of this chapter focuses on discrete profiles which are repeated in a periodic fashion to allow for ensemble averaging. These profiles are periodic, repeated in time, but discrete in the sense that the airfoil vanes are statically held at a constant position long enough for any transient effects to settle out before the next dynamic motion is applied. One of these discrete profiles discussed in the following section was impulse profiles, or creating a short change in tunnel speed before returning to steady state speed. These impulse profiles are defined to have the form of a theoretical $1 - Cosise$ shaped gust which is of particular interest because FAR 25 [5], which specifies aircraft gust loading requirements.

The first impulses investigated involved commanding the vanes to follow a $1 - Cosine$ shaped profile in the airfoil vane angle. Four different impulses were performed, an amplitude of 45° for an open-closed-open pulse, or velocity lull, an amplitude 45° closed-open-closed pulse, or velocity gust, an amplitude 90° lull, and an amplitude 90° gust. These cases are presented in Figures 4.9, 4.10, 4.11, and 4.12. Each case was performed with a one, and two second pulsewidth. All of these gusts were performed at motor speeds of $n = 318$ and 600 RPM which correspond to $U_\infty|_{\theta=0^\circ} = 10$ m/s and 20 m/s respectively. The impulses were repeated every 10 seconds, which after reviewing data was sufficient time for transient effects to settle out between pulses. Data from both the hotwire and encoder measurements were ensemble averaged over these 20 pulses to find an average profile. For comparison between different velocities, the magnitude of the velocity was normalized by the fully open test section speed, $U_\infty|_{\theta=0^\circ}$. Normalized velocity profiles for each pulsewidth are presented in the aforementioned figures.

Several things are to be noted from this initial set of pulses. First is the asymmetry between the vanes opening and closing. When the vanes are closing, the velocity responds fairly quickly. However as the vanes are opened, there is a longer settling time as the flow re-accelerates. This suggests that the tunnel has two separate time constants for accelerating and decelerating the flow.

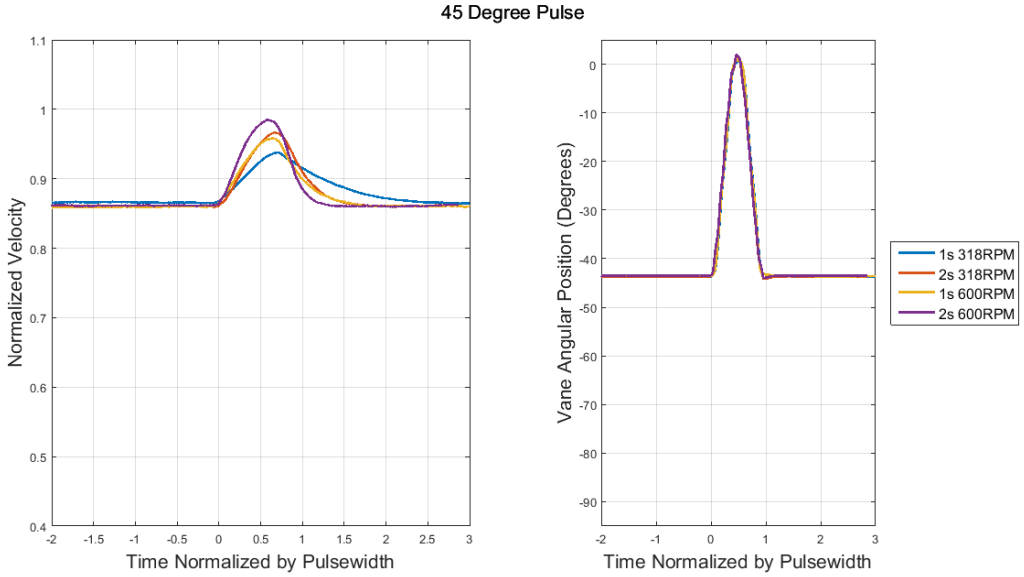

Figure 4.9: Normalized velocity profiles for 45° amplitude 1 – *Cosine* opening (gust).

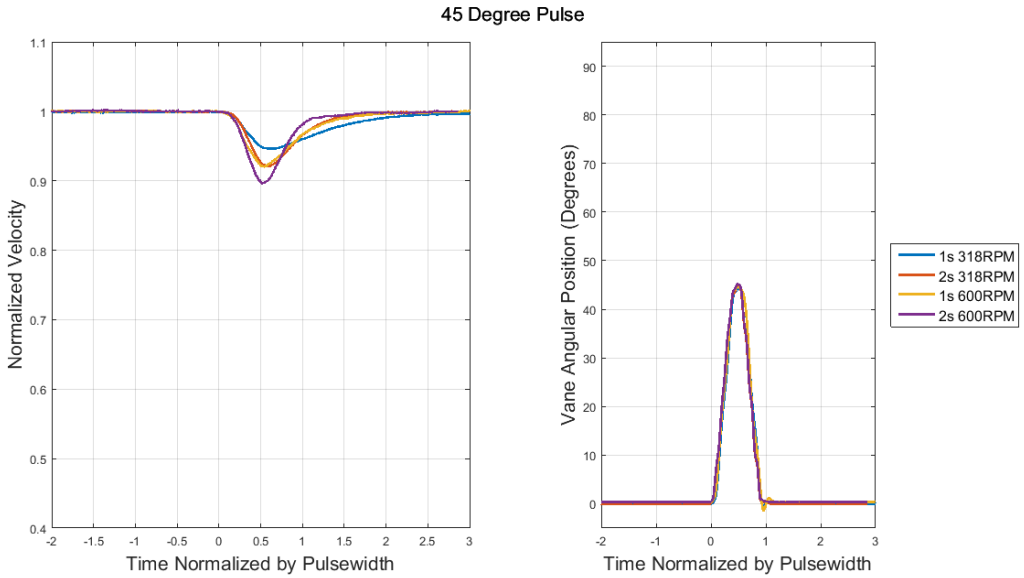

Figure 4.10: Normalized velocity profiles for 45° amplitude 1 – *Cosine* closing(lull).

This has not been shown in the previously derived mathematical model, but has been accounted for in previous systems with the shapes of vane angle profiles generated to control test section speed. This settling time is dependent on test section speed, with the faster test section speed settling faster. The amplitude of the impulse is also dependent on the test section speed. This is

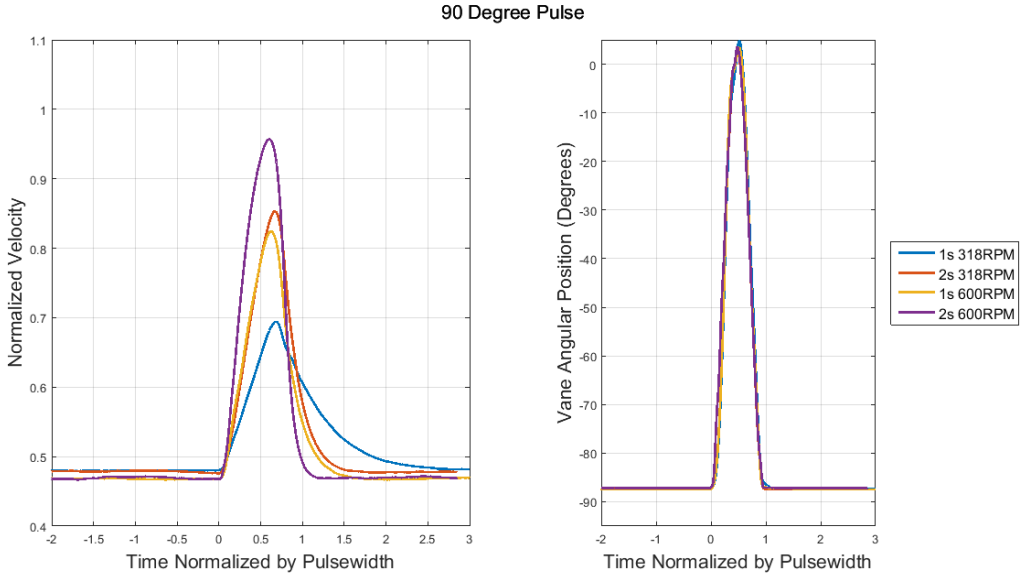

Figure 4.11: Normalized velocity profiles for 90° amplitude $1 - Cosine$ opening (gust).

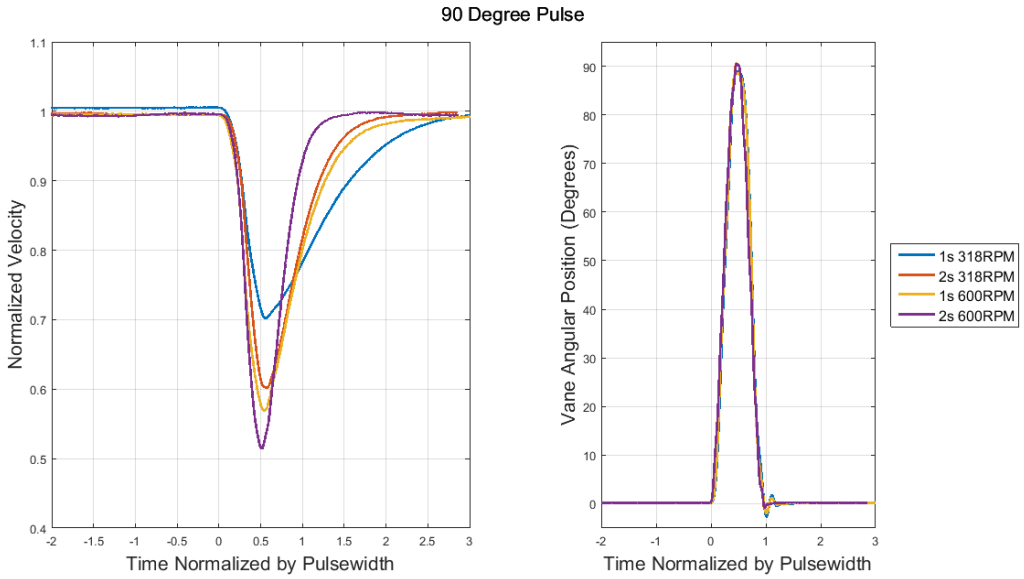

Figure 4.12: Normalized velocity profiles for 45° amplitude $1 - Cosine$ closing (lull).

consistent with the mathematical model, as the tunnel time constant is inversely proportional to test section speed. An interesting phenomenon to note is how the profiles for a $T = 2$ s pulse at $U_\infty|_{\theta=0^\circ} = 10$ m/s and the $T = 1$ s pulse at $U_\infty|_{\theta=0^\circ} = 20$ m/s collapse to nearly the same profile. The profiles are very similar, and this phenomenon is seen in several other tested profiles.

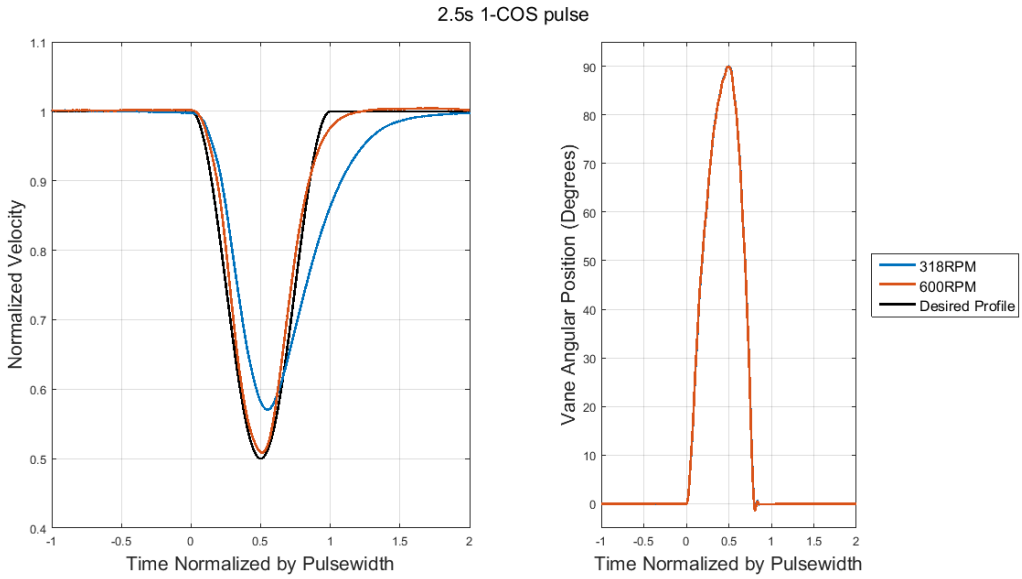

Figure 4.13: Normalized velocity response for a modified $1-Cosine$ profile with a $T = 2.5$ s period impluse.

The next profile of interest was producing a $1-Cosine$ shaped pulse in the test section speed. To do this, in the same manner as the continuous profiles, using the static data a profile was created to match the desired reduction in speed to a vane angle. The difference in time constants was also taken into consideration. From the ramp data, it was noted that the settling time for both a half second ramp and one second ramp from fully closed to open was about 1.25 seconds. It was decided to use a profile which closed the inlet over 1.25 seconds, and then reopened in.75 seconds. For a slower profile which could be assumed to be near steady state, the ramp up and ramp down were allowed to be the same time. Again judging from the ramp data, a time of 3 seconds was near steady state, so a 6 second pulse was created. Figures 4.13 and 4.14 present these modified $1-Cosine$ profiles.

The two profiles both are similar to the desired pulse in velocity. As with the continuous profile, the asymmetry in the input allowed for the tunnel to respond with a similar acceleration and deceleration to the desired profile. The dependence on speed is again seen, with the profiles at $n = 600$ RPM motor speed matching closer to the desired profile and showing a smaller phase

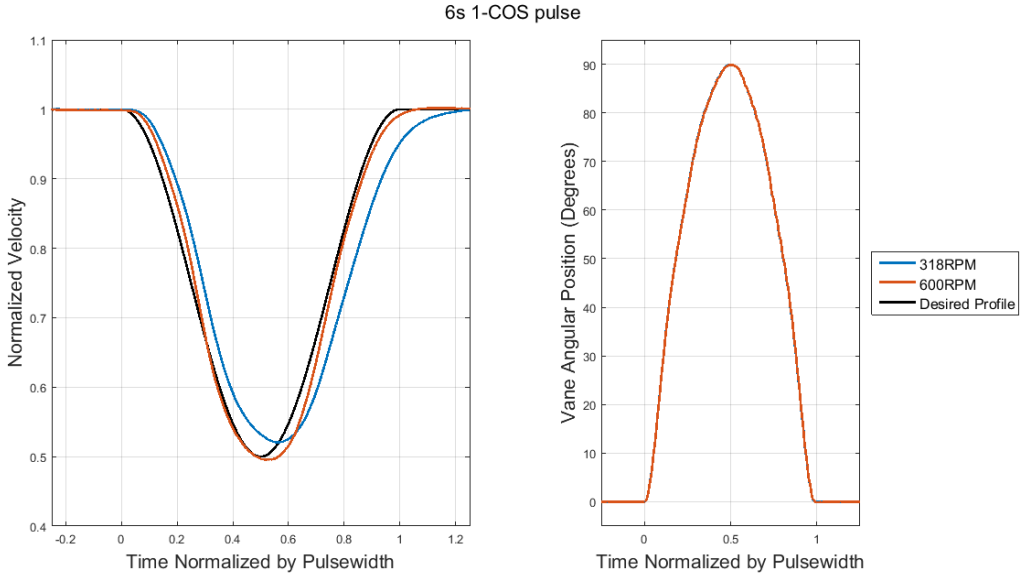

Figure 4.14: Normalized velocity response for a modified $1 - Cosine$ profile with a $T = 6$ s period impluse.

delay. The longer, six second, pulse showed symmetry, demonstrating that it was sufficiently close to steady state.

Another data set was taken to investigate how the amplitude of the impulse approaches that of a steady state closure and is presented Figure 4.15. The amplitude approaches that of the steady state as the pulse-width increases. Pulse-widths greater than 4 seconds have amplitudes near that of steady state and increase in pulse-width show no difference in amplitude.

4.2.3 Ramps

The other type of periodic discrete profile which was investigated was a ramp profile. The commanded profile was trapezoidal in shape, going from an initial position to a final position linearly over a specified time, remaining at the position for enough time for any transient effects to settle, and back to the initial position over the same time period. These ramps were performed at amplitudes of $A = 45°$ and $90°$ for an acceleration time of one half, one and five seconds. Tests were performed at motor speeds of $n = 318$ and 600 RPM. The profiles were normalized by open test section velocity and acceleration time.

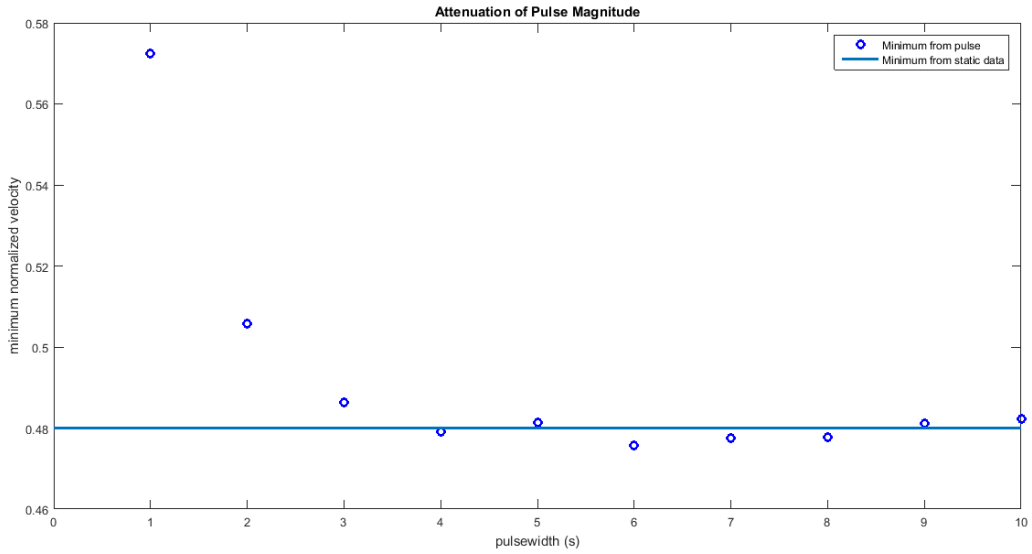

Figure 4.15: Impulse Amplitude versus Pulse-width

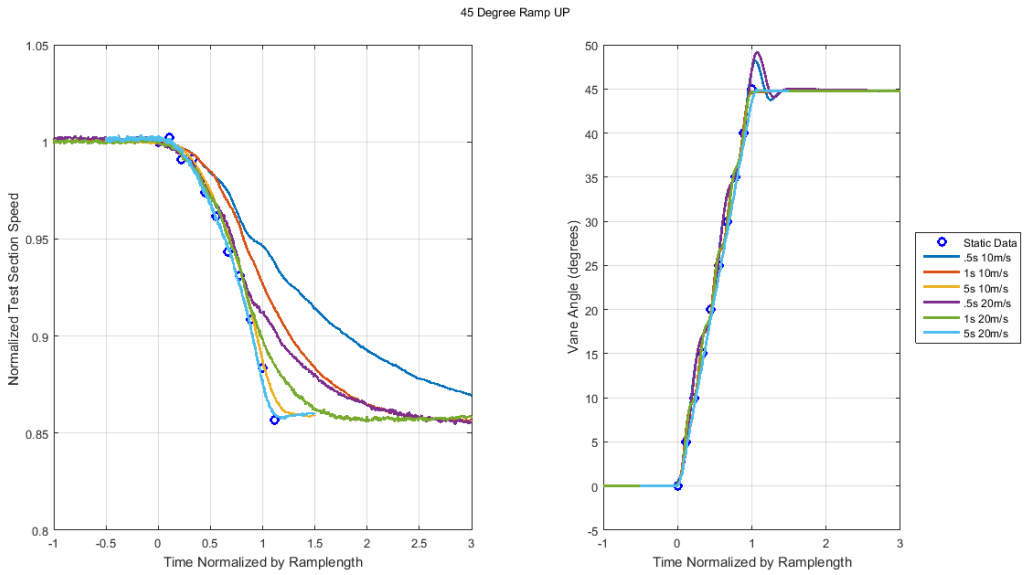

Figure 4.16: Normalized velocity profiles for 45° amplitude ramp closing (lull) and $n = 318$ RPM.

At 600 RPM ramps were performed at ramp acceleration times of one to ten seconds with 1 second increments to investigate how the profiles approach the static data. These results are included in Figures 4.20 and 4.21.

The data shows the expected trend, as the acceleration time increases and the angular speed

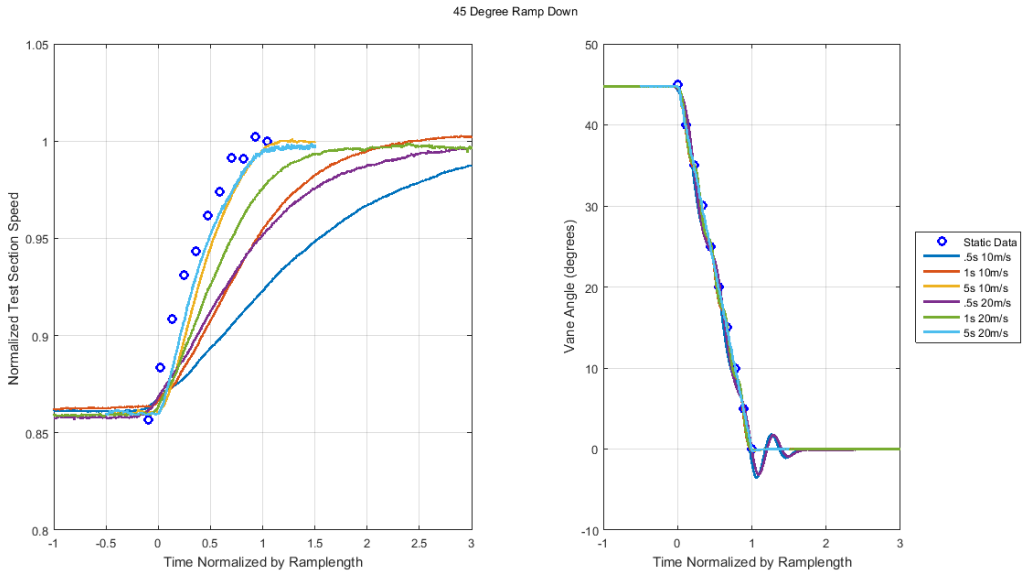

Figure 4.17: Normalized velocity profiles for 45° amplitude ramp opening (gust) and $n = 318$ RPM.

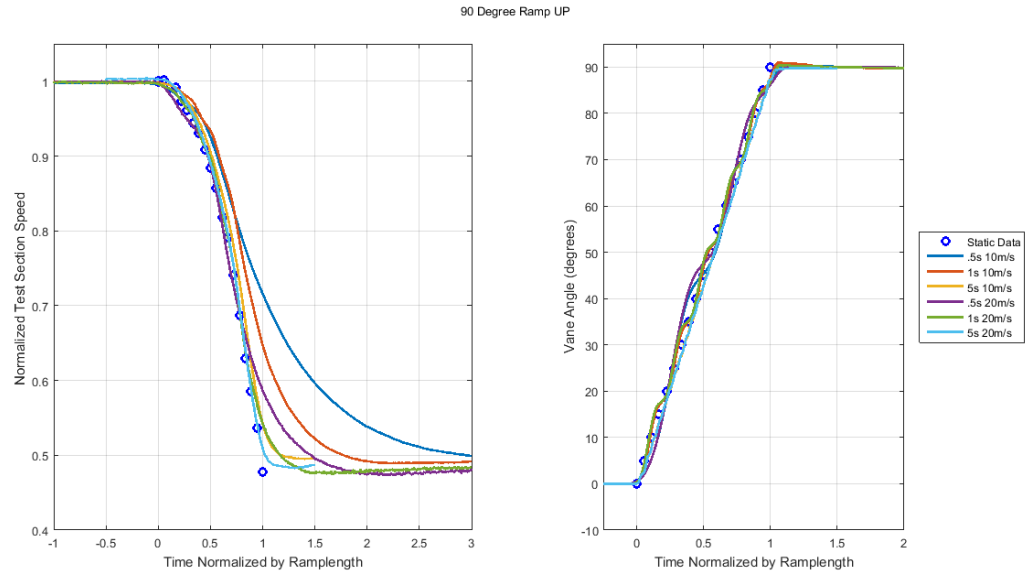

Figure 4.18: Normalized velocity profiles for 90° amplitude ramp closing (lull) and $n = 318$ RPM.

of the vanes approaches zero, the velocity approaches that of the static measurements. For the 600 RPM case, the acceleration time of $T = 4$ s or longer seem to be sufficiently close to the steady state data and increases in acceleration time provide minimal improvement of the profile. This is finding is fairly similar to the the finding with the discrete pulses

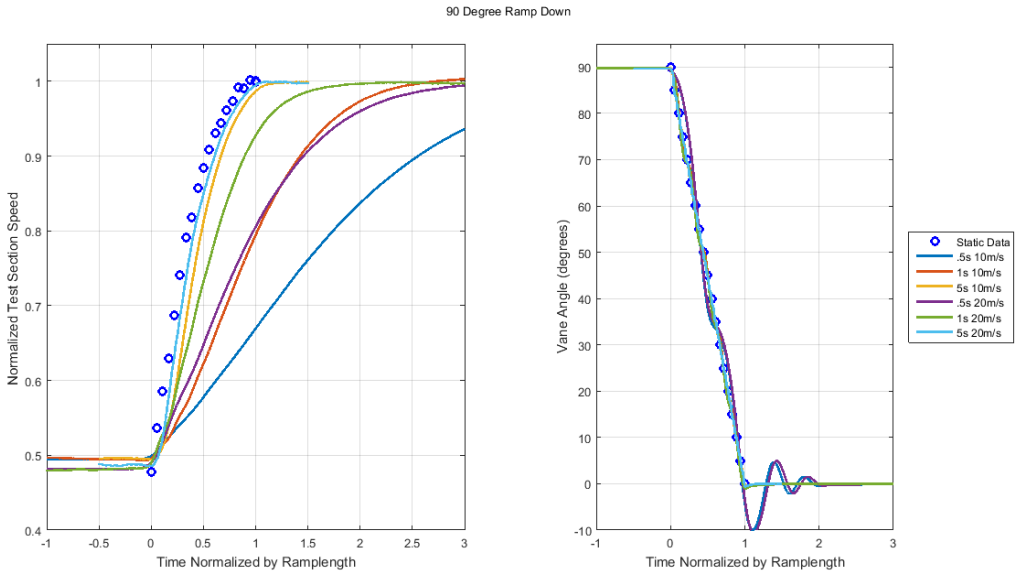

Figure 4.19: Normalized velocity profiles for 90° amplitude ramp opening (gust) and $n = 318$ RPM.

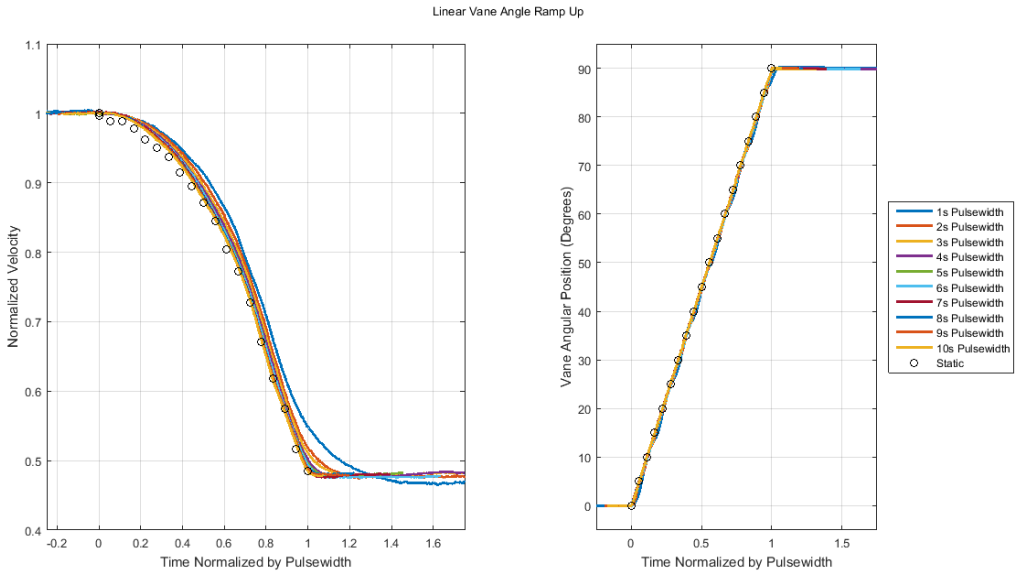

Figure 4.20: Normalized velocity profiles for 90° amplitude ramp closing (lull) and $n = 600$ RPM.

Next a custom profile was created to try to achieve a linear increase and decrease in test section speed, where a similar technique was used as previously discussed for the impulse. The effect of velocity was initially ignored for creating this polynomial for simplicity, as the effect of test section speed on static velocity reduction is fairly small. The results are presented in Figures 4.22

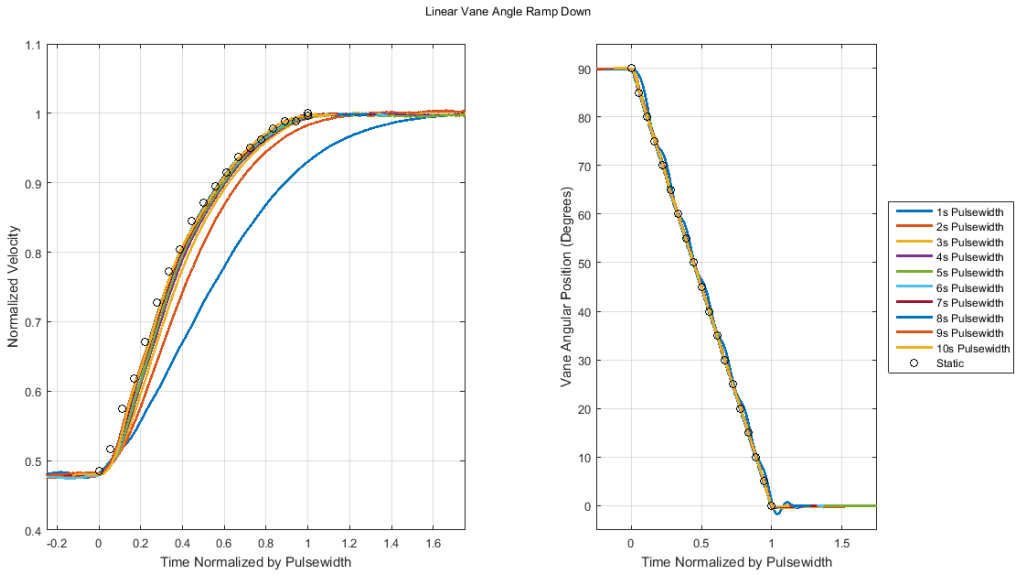

Figure 4.21: Normalized velocity profiles for 90° amplitude ramp opening (gust) and $n = 600$ RPM.

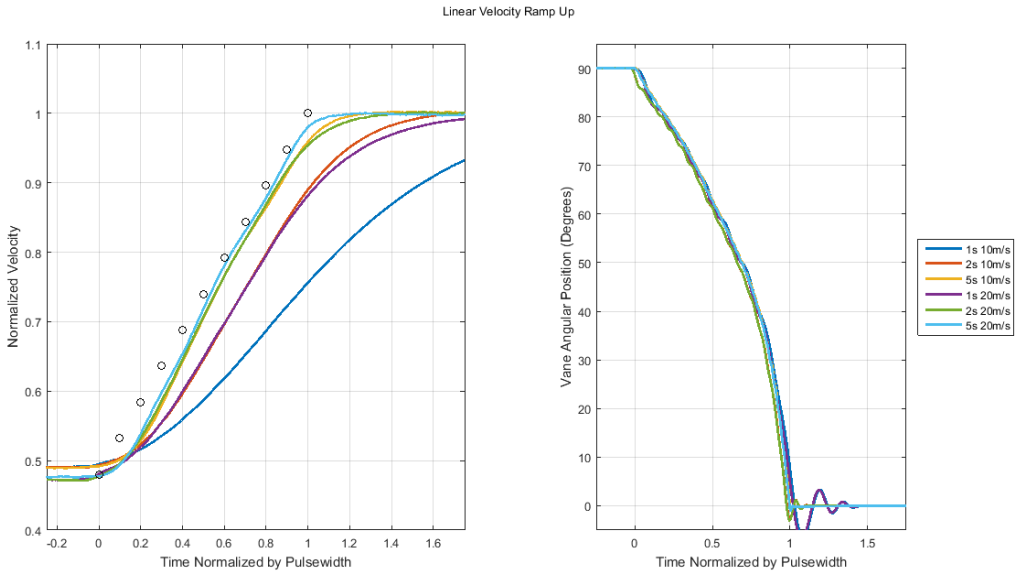

Figure 4.22: Normalized velocity response for a modified ramp profile to produce a linear velocity deceleration.

and 4.23.

A fair amount of success was attained in creating the linear profile. The five second ramps all appeared to converge to the desired profile. As the ramp length decreases, there remains a portion

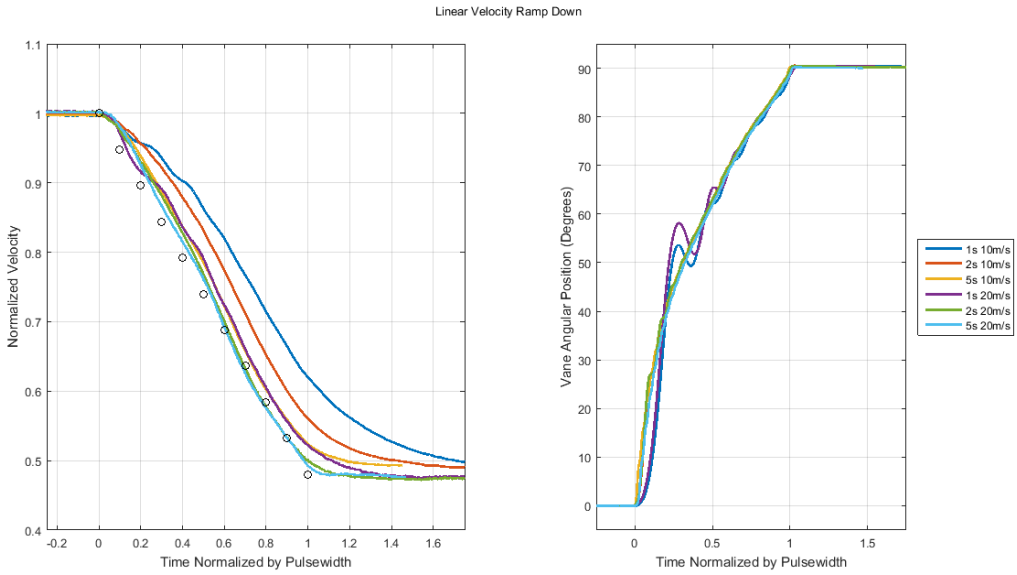

Figure 4.23: Normalized velocity response for a modified ramp profile to produce a linear velocity acceleration.

of the profile which is linear, but there is an increasing degradation of the linear profile due to the wind tunnels limited time response. Consistent with previously discussed findings, closing the inlet area (decreasing velocity) produces a profile closer to the desired profile and opening the inlet area (increasing velocity) shows faster time response. Looking at the encoder data, there is an overshoot and recovery to the profile in the one second opening pulse, suggesting that the motor is torque limited and has trouble maintaining the fast dynamic profiles.

4.2.4 Gust Speed

Comparing the front and rear hotwire signals allows for an estimate of the speed at which the gust propagates through the test section. One way of doing this is comparing the Fourier transforms of the front and rear hotwires, and comparing the phase delay between the signal. This technique is best applied to the continuous periodic (sinusoidal) profiles and results are shown below.

What can be seen here is a dependence on test section speed. The velocities are all on the order of the speed of sound, and at least an order of magnitude higher than the test section speed. For $U_\infty|_{\theta=0^\circ} = 10$ m/s most of the results average to a gust propagation speed of approximately

Table 4.1: Lists the estimated gust speed from the sinusoidal oscillations in test section speed versus the wind tunnel motor speed, n, and oscillation frequency, f.

Motor Speed (RPM)	Frequency (Hz)	Mean Gust Velocity (m/s)
318	.4	161.4
600	.4	353.9
318	.2	157.7
600	.2	299.9

Table 4.2: Lists the estimated gust speed from the sinusoidal oscillations in vane angle versus the wind tunnel motor speed, n, and oscillation frequency, f.

Motor Speed (RPM)	Frequency(Hz)	Mean Gust Velocity (m/s)
318	1	408.1
600	1	373.5
318	.5	174.5
600	.5	389.9
318	.2	176.2
600	.2	360.3

160 m/s. For $U_\infty|_{\theta=0^\circ} = 20$ m/s the results average to a gust propagation speed of approximately 360 m/s. This is above the calculated speed of sound at the time of these tests, this may be due to the slower sampling rate of these tests as they were not originally intended for this test. The data show that there is a dependence on mean test section speed.

A second method involved impulses. A code was written to find to displace the front hotwire signal and calculate an error from the rear hotwire signal, and continue to displace the signal until a minimum error is found. Knowing the sampling rate, the displacement, in samples, can be transformed into a time delay between the signals, and then into a gust speed. Data was collected at motor speeds of $n = 318$ and 600 RPM at s sampling rate of 10,000 samples per second.

This showed results much closer to the speed of sound, as well as showing less dependence on open test section speed. Though the means converge close to the speed of sound, the large standard deviation of the sample indicates that a more precise measurement and post processing technique

Table 4.3: Lists the estimated gust speed from the discrete 1 second 90 degree pulses versus the wind tunnel motor speed.

Motor Speed (RPM)	Gust speed(m/s)	standard deviation (m/s)
318	270.1	43.87
600	310.8	36.78

should be used to confirm this.

4.3 Time Response of tunnel

Using the data from ramps and impulses the time response of the system can be modeled. The first order approximation of the system can be written as the following:

$$\tau\epsilon' + \epsilon = f(t) \tag{4.1}$$

where ϵ is the fluctuation from the mean flow normalized by the open test section speed at a set blower speed, τ is the time constant, and $f(t)$ is a function based on the desired normalized velocity fluctuation. The time constants for the first order approximation can be estimated using the time delay in tracking a linear ramp. The solution for tracking a linear ramp with slope m for a first order system is

$$\epsilon(t) = m(t - \tau) * e^{\frac{-t}{\tau}} \tag{4.2}$$

From the data of a linear ramp in velocity the time delay between the desired signal and the velocity response is the time constant, τ, The time constant was put in the form previously discussed, as an empirical constant multiplied by a length, here the test section length, divided by test section speed.

These time constants appear to make sense in light of the previous results, with the time constant dependent on test section speed and that there is a difference in time response when accelerating or decelerating the flow. For a comparison with the experimental results the data presented in Figures 4.18 and 4.19 was used. The encoder data was used to define $f(t)$ based

Table 4.4: Estimates of wind tunnel time constants from linear ramps of tests section speed

Accelerative Time Constant	Decelerative Time Constant
$\tau = 1.27 * L_t/U_\infty$	$\tau = .899 * L_t/U_\infty$

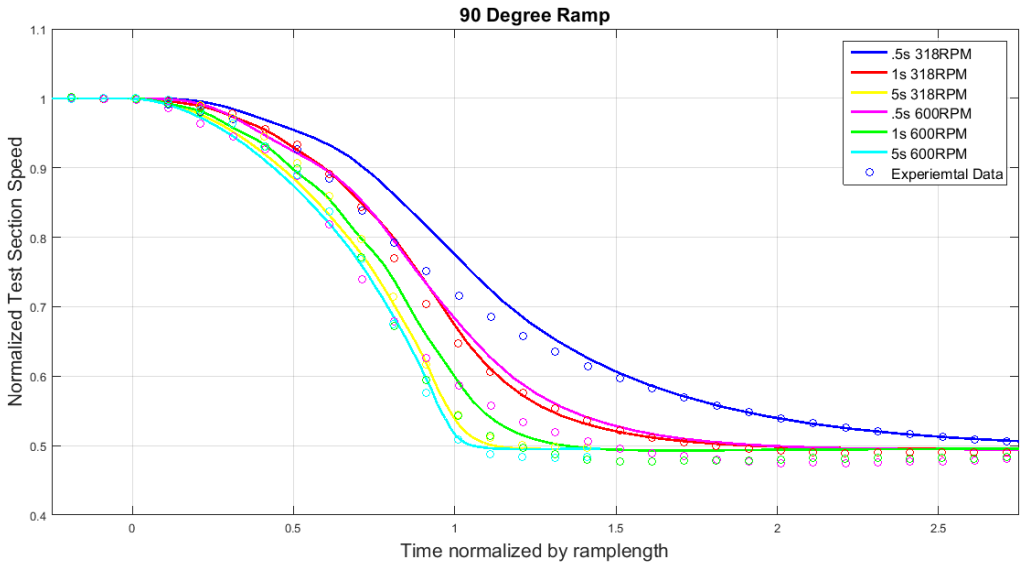

Figure 4.24: Comparison of the predicted wind tunnel time response versus the experimental results for a decelerative ramp profile.

on the static data. The first order equation was then solved in time using MATLABs ODE45. Figures 4.24 and 4.25.

The data shows the correct trends, but does not match the individual profiles very well. The decelerative ramp shows settling times which match the experimental data, while with the accelerative ramp the model tended to under predict the settling time. This suggests that perhaps the time constant calculated from the linear velocity ramps was too low. The same technique was used to look at an impulse. A 90° impulse with a period of $T = 1$ and 2 s at motor speeds of $n = 318$ and 600 RPM were examined. The experimental results were shown in Figure 4.12, and the comparison with the first order model is presented in Figure 4.26.

The model tends to under predict amplitude and settling time for the dynamic motions.

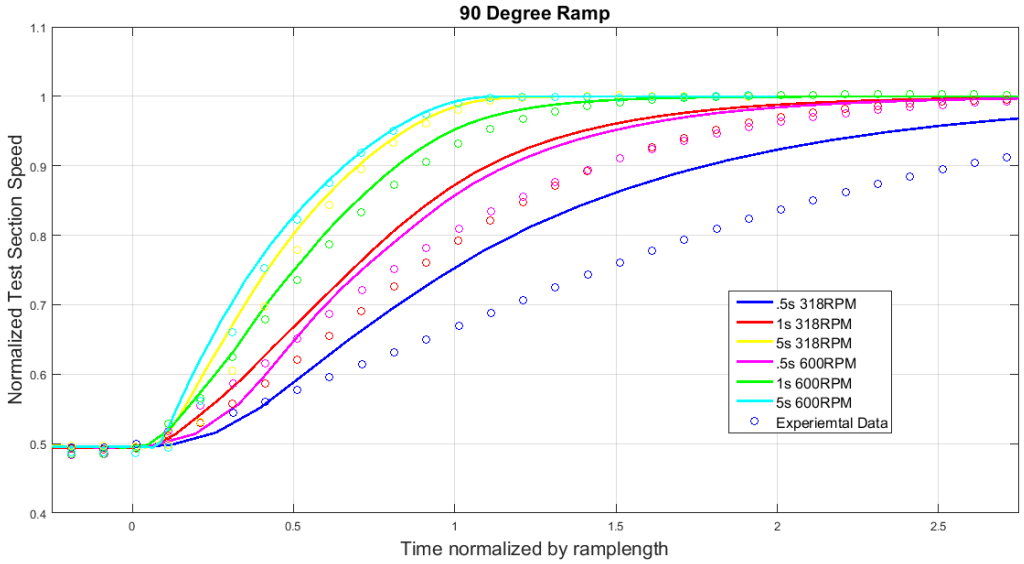

Figure 4.25: Comparison of the predicted wind tunnel time response versus the experimental results for a acelerative ramp profile.

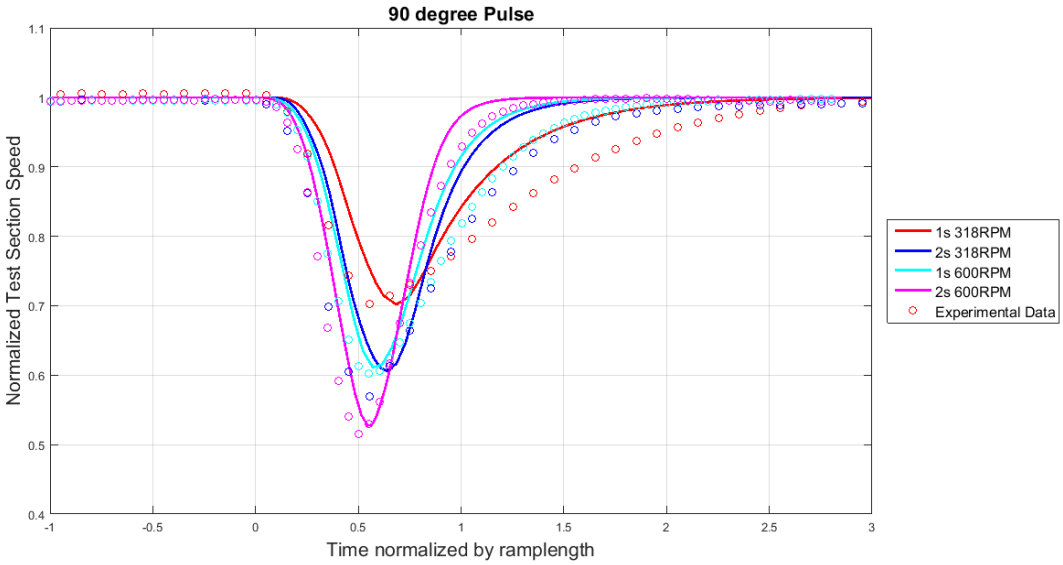

Figure 4.26: Comparison of the predicted wind tunnel time response versus the experimental results for a decelerative impulse profile.

However the model captures many of the effects previously noted. The profiles for pulses and ramps at $n = 318$ RPM are similar to those at $n = 600$ RPM with half of their characteristic time. The amplitudes increase with increases open tests section speed and normalized settling

times decrease.

The differences in the model prediction and experimental data are significant enough to suggest that the system is not a linear first order system. The model does suggest however, that the tunnel time constant is inversely proportional to the open test section speed. This finding was also shown by Greeblatt [6]. The difference in time constants for accelerating and decelerating flow has not been discussed in the previous literature and provides an opportunity for further investigation.

Chapter 5

Conclusions

In conclusion, a gust generation system was successfully designed and installed on the inlet of the CU Boulder Low speed wind tunnel. The system shows potential in creating several gust shapes and amplitudes.

The static qualification showed a reduction in test section speed to 48% of the open test section speed. The reduction followed different profiles depending on if the vane angle was positive or negative, but the asymmetry was shown to be a result of the asymmetric reduction of inlet area, and ultimately the reduction of test section speed was a function of inlet area. Despite the side to side asymmetry, opening and closing the vanes showed no hysteresis for static position holds. The reduction was also dependent on the open wind tunnel speed, with higher open speeds seeing slightly larger speed reductions.

The unsteady performance tests showed that the wind tunnel responds differently when the inlet area is reduced and when it is increased. Accelerating flow had slower time responses that decelerating flow. This means that for profiles to create a symmetric rise and fall in speed, such a $1 - Cosine$ impulse or continuous sinusoidal oscillations, the input position signal will need to account for this difference in time response. This ultimately puts a limit on the types of disturbances which can be created and their timescales. The slower time response of the accelerating flow determines the minimum period, or maximum frequency that can be generated. The time response of the tunnel was shown to be inversly proportional to speed, as predicted by the mathematical techniques defined by Greenblatt [6].

The speeds at which the disturbances moved through the test section were calculated for both continuous and discrete disturbances. For continuous sinusoidal oscillations the phase speed of the disturbances was of at least an order of magnitude higher than the mean test section speed. The phase speed also appeared to have a dependence on mean test section speed. For discrete impulses there appeared to be less dependence on mean test section speed, and for both speeds tested the gust propagated through the test section close to the speed of sound. This suggests that the disturbances generated within a closed test section act a global disturbances.

5.1 Recommendations for Future Work

There are several modifications that can be made to the system which could improve its performance. The first of which is adding a bounding wall to either side of the vanes. This would cause the positive and negative vane angles to reduce the inlet area symmetrically as well as prevent flow around the sides of the vanes. This would also allow the system to create the same disturbances in test section speed regardless of whether the vane angle is positive or negative. Another modification to the system would be improving motor performance. There is a following error in may of the position signals, often seen as a deviation from the desired profile with a dominant frequency around 5Hz. This can be improved through improvements in motor tuning, which was done after the problem was initially discovered. The faster profiles presented in this work approached the peak torque of the motor, so for faster profiles a more powerful motor, or increased gear ratio, would be necessary.

While the tests preformed provided an initial insight into the response of the tunnel there are several more tests which can give further insight. The asymmetry between vanes opening and closing can be investigated more, over a wider range of frequencies or pulse widths. This can lead to the creation of several more profiles for continuous sinusoidal oscillations of speed and $1-Cosine$ gusts. Further investigation into gust propagation speed can be preformed. The data presented was only for a small number of frequencies at only two set speeds. Taking a large data set over multiple frequencies at several speeds will help determine more accurately how the disturbance

advects through the test section. Larger sets of discrete pulses can also be preformed to confirm that the pulses move through the test section close of the speed of sound, regardless of the mean test section speed. Repeating these tests with the test section removed was beyond the scope of this work, but the system is fully capable of investigating these phenomena with the test section removed. With the system qualified the facility can test a variety of unsteady phenomena in the wind tunnel.

Bibliography

[1] Daniel P. Brzozowski, John R. Culp, Ali T. Kutay, and Ari Glezer Jonathan A. Muse. Closed-loop aerodynamic flow control of a free airfoil. In 4th Flow Control Conference, Seattle, Washington, 23 - 26 June, 2008.

[2] G. Charnay and J. Mathieu. Periodic flow in a wind tunnel produced by rotating shutters. Transactions of the ASME June, 1976.

[3] Genevieve Comte-Bellot and Stanley Corrison. The use of a contraction to improve the isotropy of grid generated turbulence. Journal of Fluid Mechanics. Vol.25 Part 4., 1966.

[4] Phillip Donely. Summary of information relating to gust loads on airplanes. Technical report, NASA, 1950.

[5] FAA. Ac no: 25.341-1. Technical report, Federal Aviation Administration, 2014.

[6] David Greenblatt. Unsteady low-speed wind tunnels. AIAA Vol 54, No. 6, June, 2016.

[7] Dustin L. Grissom and William J. Davenport. Development and testing of a deterministic disturbance genrator. In 10th AIAA/CEAS Aeroacoustics Conference, 2004.

[8] K. Grunland, B. Monnier, M. Ol, and D. Williams. Airfoil longitudinal gust response in seperated vs attached flows. Physics of Fluid 26, 2014.

[9] Wilmer H. Reed III. Aeroelasticity matters: Some reflections on two decades of testing in the nasa langley dynamics tunnel. In Intern. Symp. on Aeroelasticity; 5-7 Oct. 1980 - 1 Oct. 1981; Nuremberg; Germany, 1981.

[10] S. Klein, D. Hoppman, P. Scholz, and R Radspiel. High lift airfoil interacting with a vortical disturbance: Wind-tunnal measurements. AIAA Journal Vol. 53, No.6 June, 2015.

[11] P.M.G.J. Lancelot, J. Sodja, and R. De Breuker. Design and testing of a low subsonic wind tunnel gust generator. In International Forum on Aeroelasticity and Structural Dynamics, 2015.

[12] Twin City Fan Comapnies LTD. Surge, stall, and instabilities in fans. Technical report, Twin City Fan Comapnies LTD, 2012.

[13] J.A. Miller and A. A. Fejer. Transition phenomena in oscillating boundary-layer flows. Journal of Fluid Mechanics Vol. 18, No. 3,, 1964.

[14] Harold N. Murrow and Kermit G. Pratt nad John C. Houbolt. Naca/nasa research related to evolution of u.s. gust design criteria. In AIAA, ASME, ASCE, AHS, and ASC, Structures, Structural Dynamics and Materials Conference; 30th; Apr. 3-5, 1989; Mobile, AL; United States, 1989.

[15] Gino Perrotta and Anya R. Jones. Transient aerodynamics of large transverse gusts and geometrically similar maneuvers. In 54th AIAA Aerospace Sciences Meeting, AIAA SciTech Forum, 4-8 January, 2016.

[16] G. Alvin Pierce. An experimental study of dynamic stall in an oscillating airstream. Technical report, School of Aerospace Engineering, Georgia institute of Technology, 1976.

[17] R. Mark Rennie, Brian Catron, M. Zubair Feroz, and David Williams. Mathematical modeling of wind tunnels for low-reynolds number unsteady aerodynamic testing. In 55th AIAA Aerospace Sciences Meeting 9 - 13 January 2017, Grapevine, Texas, 2017.

[18] S. Ricci and A. Scotti. Wind tunnel testing of an active controlled wing under gust excitation. In 49th AIAA/ASME/ASCE/AHS/ASC Structures, Structural Dynamics and Materials Conference, 7-10 April, 2008.

[19] Jason M. Roadman and Kamran Mohseni. Gust characterization and generation for wind tunnel testing of micro aerial vehicles. In 47th AIAA Aerospace Sciences Meeting Including the New Horizons Forum and Aerospace Exposition 5-8 January, 2009.

[20] AJ Saddington, MV Finnis, and K Knowles. The characterization of a gust generator for aerodynamic testing. Journal of Aerospace Engineering, 2014.

[21] W.S. Saric, S. Takagi, and M. Mousseux. The asu unsteady wind tunnel and fundamental requirements for freestream turbulence measurements. In AIAA 26th Aerospace Sciences Meeting, 1988.

[22] D. M. Tang, Paul G. A. Cizmas, and E. H. Dowell. Experiments and analysis for a gust generator in a wind tunnel. Journal of Aircraft Vol. 33 No.1 January - February, 1996.

[23] Deman Tang and Earl H. Dowell. Experimental and theoretical study of gust response for high-aspect-ratio wing. AIAA Journal Vol.40, No.3 March, 2002.

[24] Kerian T. Wood, Ronald M. Cheung, Thomas Richardson, and Jonathan Cooper. A gust generator new design for a low speed wind tunnel: Design and commissioning. In 55th AIAA Aerospace Sciences Meeting, AIAA SciTech Forum, 9-13 January, 2017.

[25] T. Wright, S. Madhavan, and J. DiRe. Centrifugal fan performance with distorted inflows. Journal of Engineering for Gas and Turbine Power, 1984.

[26] ZhiGang Wu and Lei Chenand Chao Yang. Study on gust alleviation and wind tunnel test. Science China Technilogical Sciences Vol. 56, No. 3 March, 2013.